Models for a stand-alone PV system

Hansen, A.D.; Sørensen, Poul Ejnar; Hansen, L.H.; Bindner, Henrik W.

Publication date:
2001

Document Version
Publisher's PDF, also known as Version of record

Risø-R-1219(EN) / SEC-R-12

Models for a Stand-Alone PV System

Anca D. Hansen, Poul Sørensen, Lars H. Hansen and Henrik Bindner

Risø National Laboratory, Roskilde
December 2000

Abstract
This report presents a number of models for modelling and simulation of a stand-alone photovoltaic (PV) system with a battery bank verified against a system installed at Risø National Laboratory. The work has been supported by the Danish Ministry of Energy, as a part of the activities in the Solar Energy Centre Denmark.

The study is carried out at Risø National Laboratory with the main purpose to establish a library of simple mathematical models for each individual element of a stand-alone PV system, namely solar cells, battery, controller, inverter and load. The models for PV module and battery are based on the model descriptions found in the literature. The battery model is developed at UMASS and is known as the Kinetic Battery Model (KiBaM). The other component models in the PV system are based on simple electrical knowledge. The implementation is done using Matlab/Simulink, a simulation program that provides a graphical interface for building models as modular block diagrams.

The non-linear behaviour of the battery, observed in the measurements, is investigated and compared to the KiBaM model's performance. A set of linear Black box models are estimated based on the battery measurements. The performance of the best linear Black box model is compared to the KiBaM model.

A validation of each of the implemented mathematical model is performed by an interactive analysis and comparison between simulation results and measurements, acquired from the stand-alone PV system at Risø.

The report has passed an internal review, performed by:

Peter Hauge Madsen	Per Lundsager

ISBN 87-550-2774-1; 87-550-2776-8 (internet)
ISSN 0106-2840
ISSN 1600-3780

Layout and Print: Danka Services International A/S, 2001

Contents

Glossary

This list contains the most important abbreviations and symbols used in the report.

Abbreviations

PV	Photovoltaic
SOC	State of charge
KiBaM	Kinetic Battery Model

Symbols

PV arrays		
I_{sc}	Short-circuit current	[A]
V_{oc}	Open-circuit voltage	[V]
V_t	Thermal voltage	[V]
e	Electron charge $e = 1.602 \cdot 10^{-19}$	[C]
I_{ph}	Photocurrent	[A]
I_D	Diode current	[A]
k	Boltzmann constant, $k = 1.381 \cdot 10^{-23}$	[J / K]
T_a	Ambient temperature	[$^\circ$C]
T_c	Cell temperature	[$^\circ$C]
G_a	Irradiation	[W/m^2]
Battery - KiBaM		
q	Total capacity	[Ah]
q_1	Available capacity	[Ah]
q_2	Bound capacity	[Ah]
$q_{\max}$	Maximum capacity	[Ah]
R_0	Internal resistance	[Ω]
E	Internal voltage	[V]
I_{bat}	Current	[A]
V_{bat}	Terminal voltage	[V]

1 Introduction

This report presents a number of models for modelling and simulation of a stand-alone photovoltaic (PV) system with a battery bank verified against a system installed at Risø National Laboratory. The work has been supported by the Danish Ministry of Energy, as a part of the activities in the Solar Energy Centre Denmark. The model of the stand-alone PV system is made up by blocks in order to facilitate the modelling of other structures of PV systems.

Many photovoltaic systems operate in a stand-alone mode. Such systems consist of a PV generator, energy storage (for example a battery), AC and DC consumers and elements for power conditioning – as sketched in Figure 1. Per definition, a stand-alone system involves no interaction with a utility grid. A PV generator can contain several arrays. Each array is composed of several modules, while each module is composed of several solar cells. The battery bank stores energy when the power supplied by the PV modules exceeds load demand and releases it backs when the PV supply is insufficient. The load for a stand-alone PV system can be of many types, both DC (television, lighting) and AC (electric motors, heaters, etc.). The power conditioning system provides an interface between all the elements of the PV system, giving protection and control. The most frequently encountered elements of the power conditioning system are blocking diodes, charge regulators and DC-AC converters.

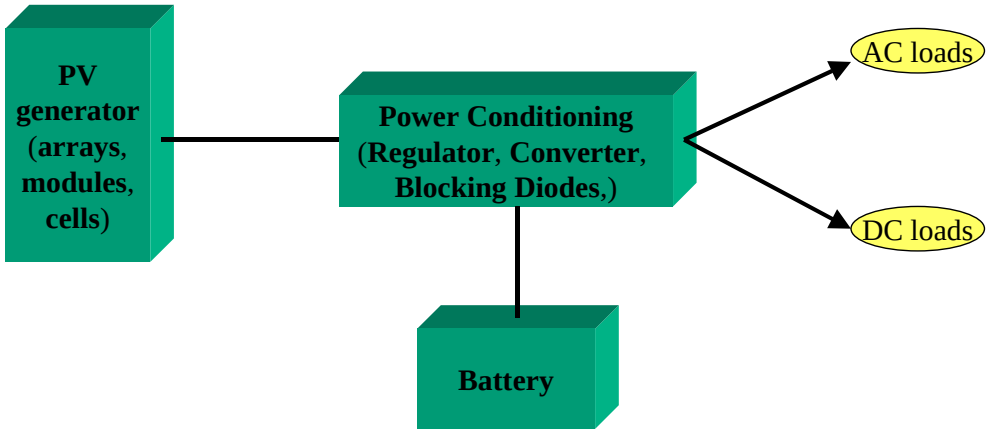

Figure 1: Elementary scheme of the components of a stand-alone photovoltaic system.

2 Description of the stand-alone PV system at Risø

The PV stand-alone system at Risø consists of two subsystems, each with its own PV arrays and controller. These two subsystems are connected in a way that they share the battery bank and load. The wiring diagram of the system is shown in Figure 2.

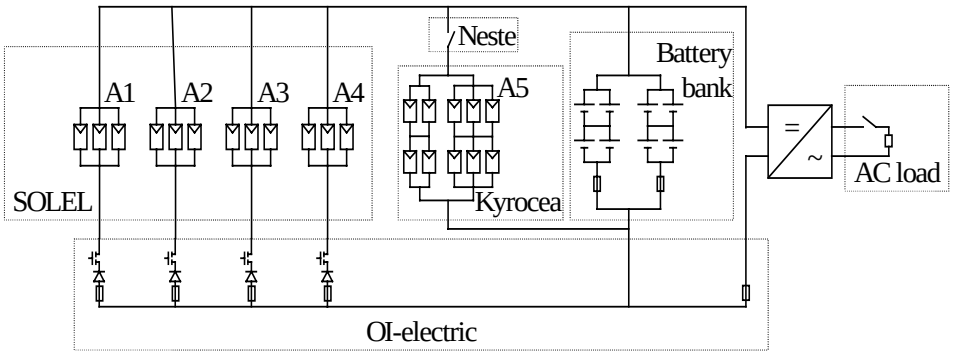

Figure 2: Wiring diagram of the stand-alone PV system at Risø.

The first PV subsystem consists of twelve 100 W monocrystalline PV modules from Solel (Denmark), i.e. this subsystem has a total rated power of 1.2 kW. The Solel modules are connected in four arrays (A1-A4), each with three modules connected in parallel. These arrays are connected to the DC bus by a microprocessor-based controller from OI-electric (Denmark), which controls the four MOSFET switches in Figure 2.

The second PV subsystem consists of ten 53 W polycrystalline solar modules from Kyocera (Japan), i.e. this subsystem has a total rated power of 0.53 kW. The Kyocera modules are connected in a single array (A5), having the same DC voltage level as the Solel arrays. The exact wiring of A5 appears from Figure 2. This array is controlled by a standard stand-alone PV system controller from Neste (Finland), which only has a single switch and consequently only supports a single array.

Both the OI-electric controller and the Neste controller have terminals for connection of batteries and loads besides the array terminals. As indicated in Figure 2, the OI-electric controller and load terminals are connected directly to battery and to AC load via an inverter, respectively. The Neste controller has battery terminals connected directly to the battery and load terminals not connected.

The battery bank is consisting of 8 lead-acid batteries 12 V/ 115 Ah. The batteries are connected in series of two modules to obtain an appropriate voltage level below the open circuit voltage of the PV arrays.

Another element shown in Figure 2 is the inverter, which transforms 24V DC to 230V AC, frequency 50 Hz. The inverter is a Victron type with 1600 W rated power, and it generates a trapezoidal waveform on the AC side.

The stand-alone system also contains an AC-load, which is a Lapell type electrical heater with 700W rated power. This heater is controlled by an on/off

thermostat. To obtain AC load in smaller steps, seven 60W bulbs have also been connected to the AC bus one by one.

Blocking diodes are used to avoid that the direction of current in the PV cells changes during the night, when the solar cells are not illuminated. In these situations, the voltage, which the solar cells produce, may be smaller than that of the battery. This will cause a discharging of the battery if the diodes are not included. The OI-electric controller provides blocking diodes on the PV array output terminals, which prevents the SOLEL arrays from leading a negative current, as shown in Figure 2. The Kyrocea panels are also blocked, but in this case, the diodes are installed in the connection box of the individual panel. These diodes are not shown in Figure 2.

Fuses are used to protect the stand-alone system against short circuit currents. The battery fuses are connected at the batteries to include protection against short circuits on the cable from the battery bank to the controller.

3 Measurement system

The measurement system is shown in Figure 3. The central unit in the measurement system is the Analog 6B ADC box. This box collects the analogue data from terminal boxes located in different places on the PV system and converts the signals to digital signals. The digital signals are transmitted on a serial connection to the data acquisition PC, where the data is logged on the harddisk.

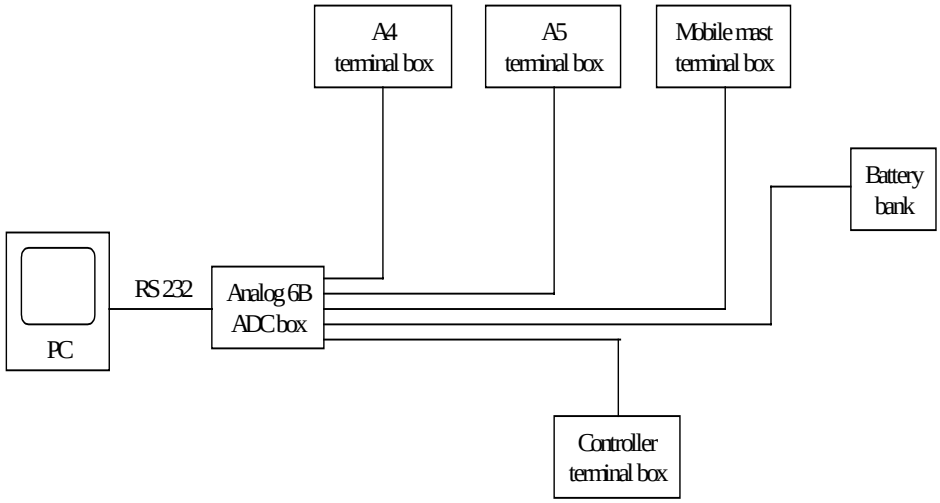

Figure 3: Block diagram for the measurement system.

The Analog 6B ADC box consists of individual Analog 6B ADC converters for each measurement channel. The 6B series supports a variety of different input ranges, from ±15 mV to ±50 V for voltage measurements and dedicated temperature ADC supporting e.g. Pt100 sensors. This enables direct connection of a variety of sensors. A power supply is built into the ADC box, and this power supply also supplies the sensors through cables parallel with the signal cables.

The PC uses Risøs own DAQ software for datalogging. The sampling frequency is set to 1 Hz, which is close to the maximum sampling rate of the setup, limited by the serial transmission between the 6B box and the PC.

The list of the sensors, which are used in the present project, are given in Table 1.

Table 1. List of sensors used in the present report.

Parameter	Symbol	Unit	Sensor type
Irradiation – array plane	G_a	W/m^2	SolData 289 pyranometer
Ambient temperature	T_a	deg C	Pt100 sensor
Battery voltage	V_{bat}	V	Direct to the ADC box
Battery current	I_{bat}	A	LEM LTA 50P/SP1
Load current	I_{load}	A	LEM LTA 50P/SP1
AC load power	P_{AC}	W	DEIF TAP-210 DG/3

4 Component models for stand-alone PV system

The main purpose of this section is to describe the models for the elements of a stand-alone PV system: PV generator, battery, controller, inverter and load. The modelling of the PV system is based on modular blocks, as illustrated in Figure 4. The modular structure facilitates the modelling of the other system structures and replacing of elements, for instance a DC load instead of an AC load.

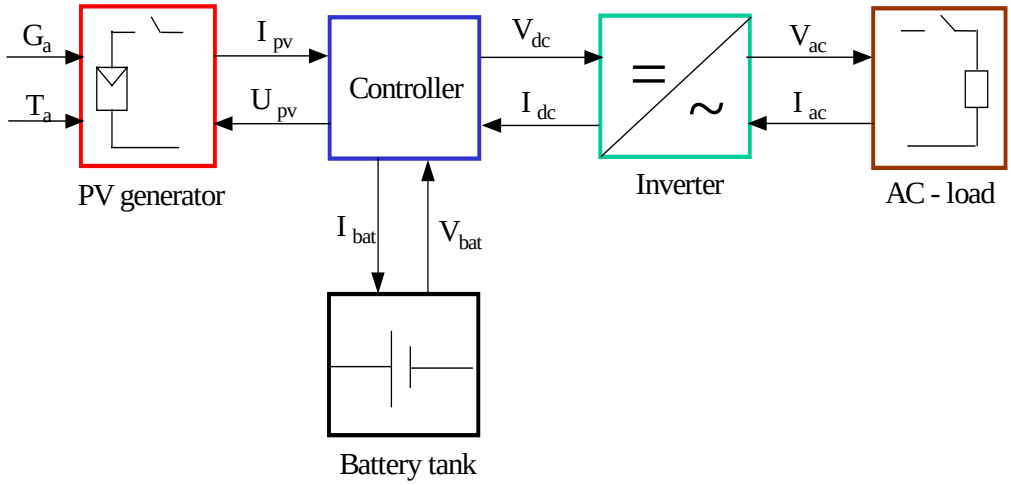

Figure 4: Block diagram for the stand-alone PV system at Risø.

4.1 PV generator (cell, module, array)

A photovoltaic PV generator is the whole assembly of solar cells, connections, protective parts, supports etc. In the present modelling, the focus is only on cell/module/array.

Solar cells are made of semiconductor materials (usually silicon), which are specially treated to form an electric field, positive on one side (backside) and negative on the other (towards the sun). When solar energy (photons) hits the solar cell, electrons are knocked loose from the atoms in the semiconductor material, creating electron-hole pairs (Lorenzo, 1994). If electrical conductors are then attached to the positive and negative sides, forming an electrical circuit, the electrons are captured in the form of electric current I_{ph} (photocurrent).

4.1.1 Solar cell model

During darkness, the solar cell is not an active device; it works as a diode, i.e. a p-n junction. It produces neither a current nor a voltage. However, if it is connected to an external supply (large voltage) it generates a current I_D, called diode current or dark current.

A solar cell is usually represented by an electrical equivalent one-diode model (Lorenzo, 1994), as shown in Figure 5.

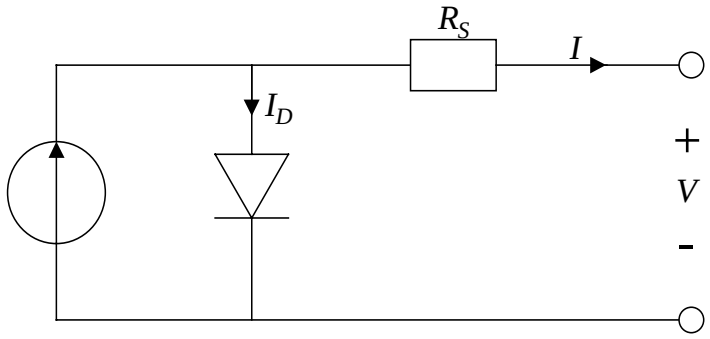

Figure 5. Model for a single solar cell.

The model contains a current source I_{ph}, one diode and a series resistance R_S, which represents the resistance inside each cell and in the connection between the cells. The net current is the difference between the photocurrent I_{ph} and the normal diode current $I_{D:}$

$$I = I_{ph} - I_D = I_{ph} - I_0\left(\exp\frac{e\,(V + IR_s)}{mkT_c} - 1\right)$$

where m is idealising factor, k is Boltzmann's gas constant, T_c the absolute temperature of the cell, e electronic charge and V is the voltage imposed across the cell. I_0 is the dark saturation current and it is strongly depending on temperature (Lorenzo, 1994).

Figure 6 shows the I-V characteristic of the solar cell for a certain ambient irradiation G_a and a certain fixed cell temperature T_c.

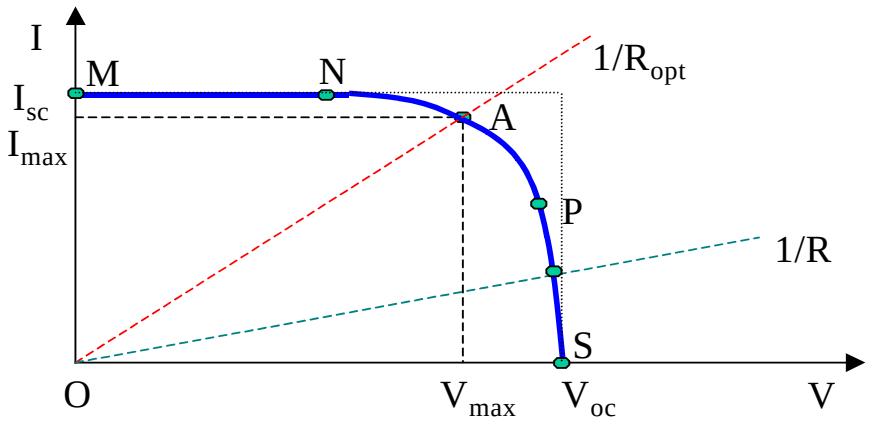

Figure 6: A typical current-voltage I-V curve for a solar cell.

In the representation of *I-V* characteristic, a sign convention is used, which takes as positive the current generated by the cell when the sun is shining and a positive voltage is applied on the cell's terminals.

If the cell's terminals are connected to a variable resistance *R*, the operating point is determined by the intersection of the *I-V* characteristic of the solar cell with the load I-V characteristic - see Figure 6. For a resistive load, the load characteristic is a straight line with a slope *I/V=1/R*. It should be pointed out that the power delivered to the load depends on the value of the resistance only. However, if the load *R* is small, the cell operates in the region MN of the curve, where the cell behaves as a constant current source, almost equal to the short circuit current. On the other hand, if the load *R* is large, the cell operates on the region PS of the curve, where the cell behaves more as a constant voltage-source, almost equal to the open-circuit voltage.

A real solar cell can be characterised by the following fundamental parameters, which are also sketched in Figure 6:

(a) Short circuit current: $I_{sc} = I_{ph}$. It is the greatest value of the current generated by a cell. It is produced under short circuit conditions: *V=0.*

(b) 0pen circuit voltage corresponds to the voltage drop across the diode (p-n junction), when it is traversed by the photocurrent I_{ph} (namely $I_D=I_{ph}$), namely when the generated current is $I = 0$. It reflects the voltage of the cell in the night and it can be mathematically expressed as:

$$V_{oc} = \frac{mkT_c}{e} \ln\left(\frac{I_{ph}}{I_0}\right) = V_t \ln\left(\frac{I_{ph}}{I_0}\right)$$

where $V_t = \frac{mkT_c}{e}$ is known as thermal voltage and T_c is the absolute cell temperature.

(c) Maximum power point is the operating point A(V_{max}, I_{max}) in Figure 6, at which the power dissipated in the resistive load is maximum: $P_{max} = I_{max} \cdot V_{max}$.

(d) Maximum efficiency is the ratio between the maximum power and the incident light power:

$$\eta = \frac{P_{\max}}{P_{in}} = \frac{I_{\max} V_{\max}}{A G_a}$$

where G_a is the ambient irradiation and A is the cell area.

(e) Fill factor is the ratio of the maximum power that can be delivered to the load and the product of I_{sc} and V_{oc}:

$$FF = \frac{P_{\max}}{V_{oc} I_{sc}} = \frac{V_{\max} I_{\max}}{V_{oc} I_{sc}}$$

The fill factor is a measure of the real *I-V* characteristic. Its value is higher than 0.7 for good cells. The fill factor diminishes as the cell temperature is increased.

In Figure 6, an *I-V* characteristic of a solar cell for only a certain ambient irradiation G_a and only a certain cell temperature T_c is illustrated. The influence of the ambient irradiation G_a and the cell temperature T_c on the cell characteristics is presented in Figure 7.

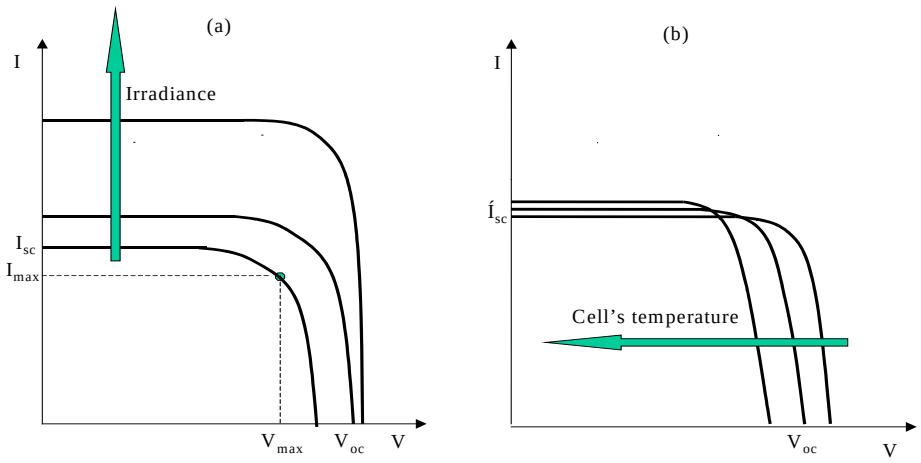

Figure 7: Influence of the ambient irradiation (a) and of the cell temperature (b) on the cell characteristics.

Figure 7(a) shows that the open circuit voltage increases logarithmically with the ambient irradiation, while the short circuit current is a linear function of the ambient irradiation. The arrow shows in which sense the irradiation and the cell temperature, respectively, increase. The influence of the cell temperature on the I-V characteristics is illustrated in Figure 7(b). The dominant effect with increasing cell's temperature is the linear decrease of the open circuit voltage, the cell being thus less efficient. The short circuit current slightly increases with cell temperature.

For practical use, solar cells can be electrical connected in different ways: series or parallel. Figure 8 presents how the I-V curve is modified in the case when two identical cells are connected in series and in parallel.

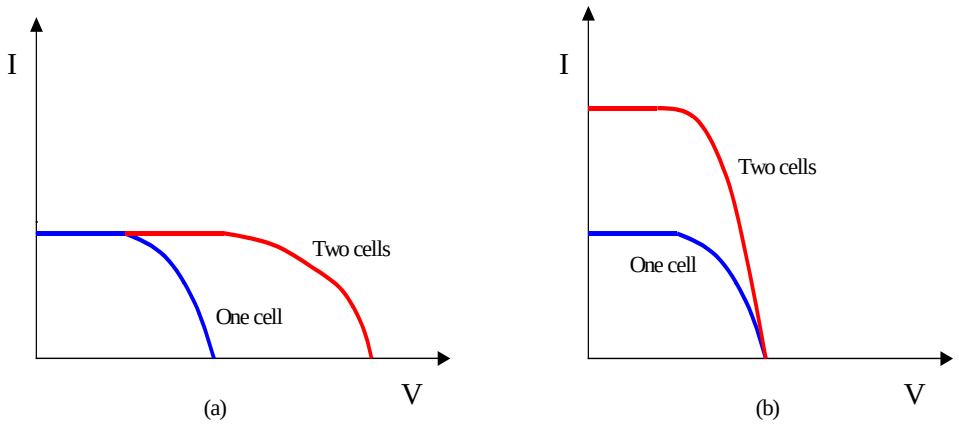

Figure 8: Series (a) and parallel (b) connection of identical cells.

It is seen that I-V characteristics of series interconnected cells can be found by adding, for each current, the different voltages of the individual cells. On the other hand, for parallel cells the currents of the individual cells must be added at each voltage in order to find the overall I-V curve.

4.1.2 Module model

Cells are normally grouped into "modules", which are encapsulated with various materials to protect the cells and the electrical connectors from the environment. The manufacturers supply PV cells in modules, consisting of N_{PM} parallel branches, each with N_{SM} solar cells in series, as shown in Figure 9.

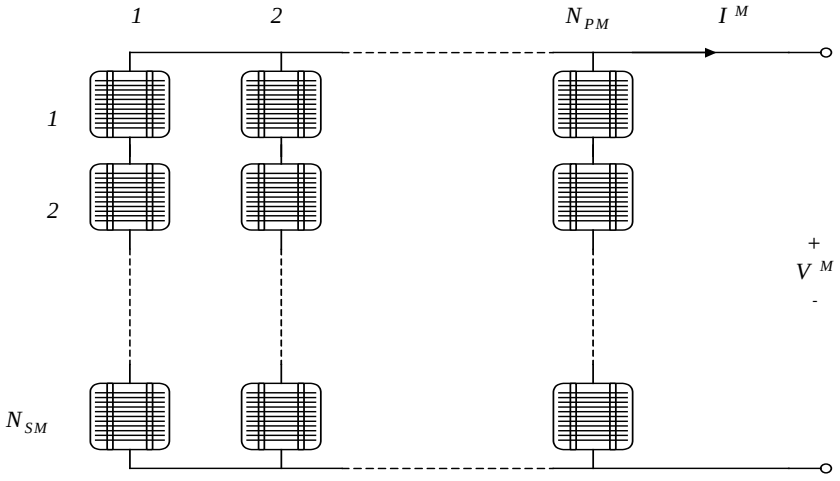

Figure 9: The PV module consists of N_{PM} parallel branches, each of N_{SM} solar cells in series.

In order to have a clear specification of which element (cell or module) the parameters in the mathematical model are regarding, the following notation is used from now on: the parameters with superscript "*M* " are referring to the PV module, while the parameters with superscript "*C* " are referring to the solar cell. Thus, the applied voltage at the module's terminals is denoted by V^M, while the total generated current by the module is denoted by I^M.

A model for the PV module is obtained by replacing each cell in Figure 9, by the equivalent diagram from Figure 5. In the following, the mathematical model of a PV module, suggested by (Lorenzo, 1994), is briefly reviewed. The advan-

tage of this model is that it can be established applying only standard manufacturer supplied data for the modules and cells. The PV module's current I^M under arbitrary operating conditions can thus be described as:

$$I^M = I_{SC}^M \left[1 - \exp\left(\frac{V^M - V_{OC}^M + R_S^M \cdot I^M}{N_{SM} V_t^C} \right) \right]$$

The expression of the PV module's current I^M is an implicit function, being dependent on:

- the short circuit current of the module, which is $I_{SC}^M = N_{PM} \cdot I_{SC}^C$
- the open circuit voltage of the module, which is $V_{OC}^M = N_{SM} \cdot V_{OC}^C$
- the equivalent serial resistance of the module, which is $R_S^M = \frac{N_{SM}}{N_{PM}} \cdot R_S^C$
- the thermal voltage in the semiconductor of a single solar cell, which is $V_t^C = \frac{mkT^C}{e}$

In current practice, the performance of a module or another PV device is determined by exposing it at known conditions. The module characteristics supplied by the manufacturer are usually determined under special conditions, as for example nominal or standard conditions (Lorenzo, 1994), see Table 2.

Table 2 Nominal and standard conditions.

Nominal conditions	**Standard conditions**
Irradiation: $G_{a,ref}$=800 W/m^2	Irradiation: $G_{a,0}$=1000 W/m^2
Ambient temperature: $T_{a,ref} = 20^\circ C$	Cell temperature: $T_0^C = 25^\circ C$
Wind speed: 1 m/s	

Under standard conditions (irradiation $G_{a,0}$ and cell temperature T_0^C), at least the following parameters are measured:

- the short circuit current for the module $I_{SC,0}^M$
- the open circuit voltage for the module $V_{OC,0}^M$
- the maximum power for the module $P_{\max,0}^M$

Under nominal (reference) conditions the following parameters are delivered:

- the ambient irradiation $G_{a,ref}$
- the ambient temperature $T_{a,ref}$
- the temperature of the cell T_{ref}^C

The whole algorithm for the computation of the current of the PV module, under certain operating points (V^M, T_a, G_a) is illustrated in Figure 10. The steps in the algorithm are as following:

1) Manufacturer's catalogues provide information about the PV module for standard conditions:
   - maximum power $P^{M}_{\max,0}$
   - short circuit current $I^{M}_{SC,0}$
   - open circuit voltage $V^{M}_{OC,0}$
   - number of cells in series N_{SM}
   - number of cells in parallel N_{PM}

2) Once the PV module's data for standard conditions are available, the next step is to compute the cell's data for standard conditions: $P^{C}_{\max,0}$, $V^{C}_{OC,0}$, $I^{C}_{SC,0}$, R^{C}_{S}, as described in Figure 10.

3) The next step is to determine the characteristic parameters of the cell under the operating conditions (V^{M}, T_a, G_a). Thus, the short circuit current of a solar cell I^{C}_{SC} is computed based on its linear dependency on the irradiation G_a:

   $$I^{C}_{SC} = C_1 \, G_a$$

   The working temperature of the cells T^{C} depends exclusively on the irradiation G_a and on the ambient temperature T_a, according to the empirical linear relation:

   $$T^{C} = T_a + C_2 G_a$$

   where the constant C_2 is computed as:

   $$C_2 = \frac{T^{C}_{ref} - T_{a,ref}}{G_{a,ref}}$$

   When T^{C}_{ref} is not known, it is reasonable to approximate $C_2 = 0.03\, C\, m^2 / W$. The open circuit voltage of the cell depends exclusively on the temperature of the solar cells:

   $$V^{C}_{OC} = V^{C}_{OC,0} + C_3 \, (T^{C} - T^{C}_{0})$$

   where the constant C_3 is usually considered to be: $C_3 = -2.3\, mV / C$.

4) Once the steps (2) and (3) are completed, the final step is to determine the module's current for operating conditions, as described in Figure 10.

MODULE DATA FOR STANDARD CONDITIONS

$$P_{\max,0}^{M},\ I_{SC,0}^{M},\ V_{OC,0}^{M},\ N_{SM},\ N_{PM} \qquad (1)$$

CELL PARAMETERS FOR STANDARD CONDITIONS

$$P_{\max,0}^{C} = P_{\max,0}^{M} / (N_{SM}\ N_{PM})$$
$$V_{OC,0}^{C} = V_{OC,0}^{M} / N_{SM}$$
$$I_{SC,0}^{C} = I_{SC,0}^{M} / N_{PM}$$

$$V_{t,0}^{C} = mkT^{C} / e$$
$$\nu_{OC,0} = V_{OC,0}^{C} / V_{t,0}^{C}$$
$$FF = (\nu_{OC,0} - \ln(\nu_{OC,0} + 0.72)) / (\nu_{OC,0} + 1)$$
$$FF_{0} = P_{\max,0}^{C} / (V_{OC,0}^{C}\ I_{OC,0}^{C})$$
$$r_{s} = 1 - FF / FF_{0}$$
$$R_{S}^{C} = r_{s}\ V_{OC,0}^{C} / I_{SC,0}^{C} \qquad (2)$$

CELL PARAMETERS FOR OPERATING CONDITIONS (V^{M}, T_{a}, G_{a})

$$C_{1} = I_{SC,0}^{C} / G_{a,0}$$
$$I_{SC}^{C} = C_{1}\ G_{a}$$
$$T^{C} = T_{a} + C_{2}\ G_{a}$$
$$V_{OC}^{C} = V_{OC,0}^{C} + C_{3}\ (T^{C} - T_{0}^{C})$$
$$V_{t}^{C} = m\,k\,(273 + T^{C}) / e \qquad (3)$$

MODULE CURRENT FOR OPERATING CONDITIONS

$$I^{M} = N_{PM}\ I_{SC}^{C}\,[1 - \exp((V^{M} - N_{SM}\ V_{OC}^{C} + I^{M}\ R_{S}^{C}\ N_{SM} / N_{PM}) / (N_{SM}\ V_{t}^{C}))] \qquad (4)$$

Figure 10: Steps in computation of PV module current, under certain operating conditions.

4.1.3 Array model

The modules in a PV system are typically connected in arrays. Figure 11 illustrates the case of an array with M_P parallel branches each with M_S modules in series.

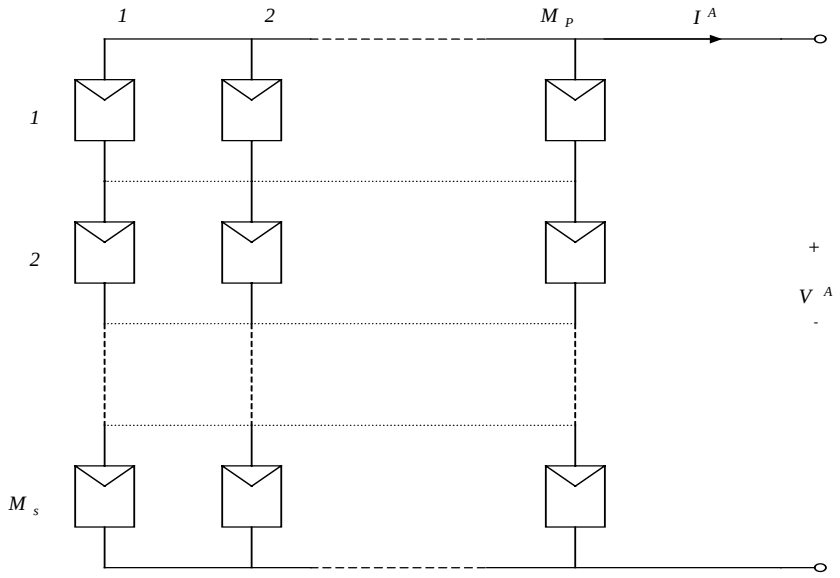

Figure 11: Solar cell array consists of M_p parallel branches, each with M_s modules in series.

The applied voltage at the array's terminals is denoted by V^A, while the total current of the array is denoted by $I^A = \sum_{i=1}^{M_p} I_i$. If it is assumed that the modules are identical and the ambient irradiation is the same on all the modules, then the array's current is:

$$I^A = M_P \; I^M$$

4.2 Battery

An another important element of a stand-alone PV system is the battery. The battery is necessary in such a system because of the fluctuating nature of the output delivered by the PV arrays. Thus, during the hours of sunshine, the PV system is directly feeding the load, the excess electrical energy being stored in the battery. During the night, or during a period of low solar irradiation, energy is supplied to the load from the battery.

4.2.1 General notions for battery

Before a mathematical model for the battery is presented, some fundamental concepts of the battery are briefly reviewed:

- **Nominal capacity** q_{max} - is the number of ampere-hours (Ah) that can maximally be extracted from the battery, under predetermined discharge conditions.

- **State of charge SOC** – is the ratio between the present capacity and the nominal capacity q_{max}: $SOC = q / q_{\max}$. Obviously 0≤ **SOC**≤1. If **SOC**=1 the battery is totally charged, otherwise if **SOC**=0 the battery is totally discharged.
- **Charge (or discharge) regime** is the parameter which reflects the relationship between the nominal capacity of a battery and the current at which it is charged (or discharged). It is expressed in hours; for example, discharge regime is 30 h for a battery 150 Ah that is discharged at 5A.
- **Efficiency** – is the ratio of the charge extracted (Ah or energy) during discharge divided by the amount of charge (Ah or energy) needed to restore the initial state of charge. It is depending on the state of charge **SOC** and on the charging and discharging current.
- **Lifetime –** is the number of cycles charge/discharge the battery can sustain before losing 20% of its nominal capacity.

Over the years a number of battery models have been developed (Facinelli, 1983), (Hyman et al., 1986), (Manwell & McGowan, 1993), (Manwell et al., 1994). Most of these models can be defined as phenomenological, namely they are based on observable quantities such as voltage, current and time, and do not depend on the internal structure of the system (Manwell et al., 1994). Other models are based on physical or electrochemical processes.

In general, the battery models view the battery as a voltage source E in series with an internal resistance R_0, as shown in Figure 12.

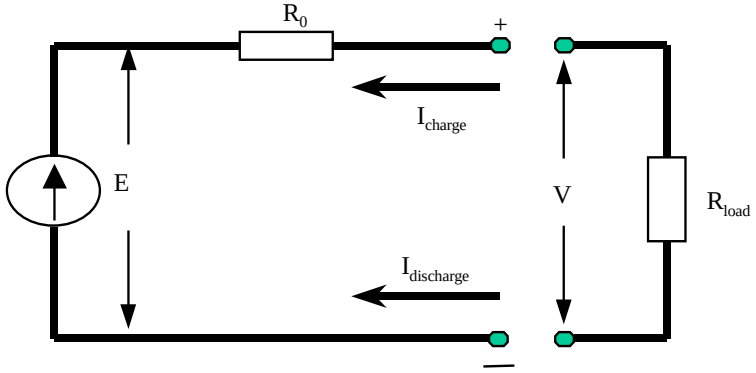

Figure 12: Schematic diagram of the battery.

The terminal voltage V is given by:

$$V = E - I\ R_0$$

4.2.2 Kinetic Battery Model (KiBaM)

This section briefly focuses on the Kinetic Battery Model (KiBaM), developed at the University of Massachusets to predict the performance of the battery, based only on manufacture's data – see (Manwell & McGowan, 1993) and (Manwell & McGowan, 1994). No extensive measurements of voltage and current are required. The main aim of the KiBaM model is to represent the sensitivity of storage capacity to the rate of discharge.

In the modelling of the battery, the convention is that the battery is seen as a generator, namely that the charge current is negative while the discharge current

is positive. The internal resistance R_0 is assumed constant. Charge is conserved under charging and discharging and the internal voltage E varies with the state of (Manwell & McGowan, 1993).

The model is composed of two major parts describing:

1) capacity model
2) voltage model.

4.2.2.1 Capacity model

The basis of this part is the assumption that some of the capacity in the battery is immediately available for the load, while the rest is chemically bound. It is helpful to imagine that the charge of the battery is held in two tanks, as in Figure 13:

- Tank 1, with width *c*, contains the available capacity (charge) q_1.
- Tank 2, with width *1-c*, contains the chemically bound capacity (charge) q_2.

Each tank has unit depth (front to the back). Notice that the combined tank area is equal to 1.
The capacity is thus reflected by the volume of a tank. The total capacity q in the battery at any time is the sum of the available capacity q_1 and bound capacity q_2. These two tanks are separated by a conductance k^1, which corresponds to the rate at which the available charge reserve is replenished from the chemical bound storage. Parameter c is a capacity ratio and corresponds to the fraction of total charge in the battery that is readily available.

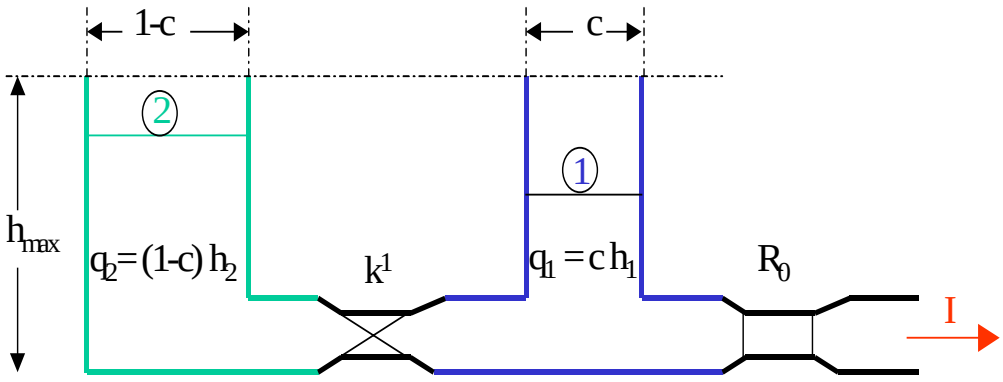

Figure 13: Schematic battery model KiBaM.

The maximum combined volume of the tanks, denoted by q_{max}, is then equal with the full head of the tanks h_{max}, namely:

$$q_{max} = q_{1,max} + q_{2,max} = ch_{max} + (1-c)h_{max} = h_{max}$$

This maximum possible capacity of the battery corresponds to the charge that may be obtained when a full battery is discharged at a very slow rate.

The head of each tank at a certain moment is given by the volume divided by the area:

$$h_1 = \frac{q_1}{c} \quad \text{and} \quad h_2 = \frac{q_2}{1-c}$$

The process by which bound charge becomes available is proportional to the difference in the head of the two tanks and depends on the rate constant k^1. This means that, if the heads of the tanks are equal ($h_1 = h_2$), there is no flow between the two tanks.

As described in (Manwell & McGowan, 1994), the flows of available and bound charge during a constant current discharge or charge are given by:

$$\begin{cases} I = -\frac{dq_1}{dt} - \frac{dq_2}{dt} \quad \Rightarrow \quad \frac{dq_1}{dt} = -I - \frac{dq_2}{dt} \\ \frac{dq_2}{dt} = k^1(h_1 - h_2) \end{cases}$$

where q_1 is available charge, q_2 is bound charge.

For simplicity, a new constant k is defined as: $k = k^1 / c(1-c)$. The model equations can thus be transformed to:

$$\begin{cases} \frac{dq_1}{dt} = -I - k\,(1-c)\,q_1 + k\,c\,q_2 \\ \frac{dq_2}{dt} = k\,(1-c)\,q_1 - k\,c\,q_2 \end{cases}$$

The eigenvalues of the system are $s = 0$ and $s = k$. Thus, one of them reflects an integrator, while the another is dependent on the value of the conductance *k*. Tank 2 can be regarded as an integrator since it is not controlled from outside.

Note that the capacity model is characterised by three constants *k*, *c*, q_{max}. These constants and the parameter R_0 can be found from manufactures discharge data or test data, by application of non-linear curve fitting methods, i.e. the non-linear least square curve fitting. In order to simplify the application of the model, it can be assumed that both in charging and in discharging the same constants are applied (Manwell & McGowan, 1993).

The parameter R_0 reflects the slope of the voltage versus current for a full battery. It is determined by extrapolating each curve "voltage versus charge removed" to zero charge removed and by computing: $R_0 = \mathrm{d}V/dI$ at time zero.

The estimation of *k*, *c*, q_{max} is performed by minimising the following criterion, expressed with the help of normalised capacities F_{t_1,t_2}:

$$error = (F_{t_1,t_2} - F_{data})^2$$

where:

1) $F_{t_1,t_2} = \frac{q_{T=t_1}}{q_{T=t_2}} = \frac{t_1 I_{T=t_1}}{t_2 I_{T=t_2}}$ represents the normalised capacity to that capacity which corresponds to the slowest discharge rate ($I_{T=t_2}$ smallest discharge current, t_2 biggest discharge time). $q_{T=t}$ denotes the discharge capacity at discharge time $T = t$ and discharge current $I_{T=t}$. t_1 corresponds to the actual discharge time, while t_2 corresponds to the biggest discharge time.

2) $F_{data} = \frac{t I_{T=t}}{t_2 I_{T=t_2}}$ represents the normalised capacity computed from data.

3) $I_{T=t} = \frac{kcq_{\max}}{1-e^{-kt} + c(kt-1+e^{-kt})}$ represents the discharge current to empty in time t a full charged battery (Manwell & McGowan, 1993).

Using the expression of the discharge current, the ratio of capacities is becoming:

$$F_{t_1,t_2} = \frac{t_1}{t_2} \frac{1-e^{-kt_2} + c(kt_2 - 1 + e^{-kt_2})}{1-e^{-kt_1} + c(kt_1 - 1 + e^{-kt_1})}$$

It is observed that the expression of F_{t_1,t_2} is only dependent on the parameters k and c, they being thus estimated by minimising the mentioned criterion. On the other hand, once k and c are determined, the maximum battery capacity $q_{\max}$ can easily be estimated by stating from the slowest discharge rate:

$$q_{\max} = \frac{I_{T=t_2}(1-e^{-k\,t_2} + c(k\,t_2 - 1 + e^{-k\,t_2})}{k\,c}$$

4.2.2.2 Voltage model

This part of the model provides the magnitude of the terminal voltage, as affected by charging and discharging to different depths at different current rates. The voltage model is able to predict that the battery voltage drops slowly (linearly) during the first part of discharge and rapidly at the end, when the battery is nearly empty.

In the KiBaM model, it is assumed that the voltage source E varies with the state of charge and current, as follows:

$$E = E_0 + A\,X + C\,X/(D - X)$$

where:

E_0 = extrapolated voltage at zero current of a fully charged battery.
A = initial linear variation of internal battery voltage with state of charge.
C, D = parameters reflecting the sharpness of end-of-discharge voltage drop (commonly called the “knee” of the curve). C will always be negative in dis-

charging. A smaller value of C gives a sharper "knee" of the discharge curve. D is positive and approximates the maximum discharge capacity.
X = normalised capacity removed from the battery at a given discharge current:

$$X = \frac{q_{out}}{q_{\max}(I)} q_{\max}$$

$q_{\max}(I)$ = capacity of the battery at each discharge current *I*. It can be found as the point in time where the voltage curve begins to drop off sharply.
$q_{\max}$ = maximum ampere-hour capacity – it corresponds to the charge that may be obtained when a battery is discharged at a very slow rate $I \approx 0$ A.
q_{out} = amount of charge that has been removed by a certain point (in discharging from a full battery):

$$q_{out} = \int I \, dt = q_{\max} - q_1 - q_2$$

The voltage model is thus characterised by four parameters E_0, A, C, D. They are also determined by the non-linear least square curve fitting methods, applied on the test data delivered by the manufacturer. In (Manwell & McGowan, 1994) it is mentioned that the voltage parameters E_0, A, C, D are best determined from separate tests for discharging and charging, while the capacity parameters k, c, q_{max} can be assumed to be the same for charging and discharging.

There are some observations on the KiBaM model, which should be noticed:

1) The normalised capacity X is always positive $X \geq 0$. It is also $X \geq q_{out}$ and $X \leq q_{\max}$.
2) In discharging, the normalised capacity X is increasing to q_{max}. Thus, the knee of the curve in discharging is produced when $D - X \to 0$, as $X \to q_{\max}$ and $D \approx q_{\max}$.
3) The term $X/(D-X)$ is always positive, and therefore the term $C\,X/(D-X)$ is negative in discharging only if $C < 0$ and positive in charging only if $C > 0$.
4) In charging of an empty battery, q_{out} can be regarded as the amount of charge that is added to charge completely the battery.
5) As in charging, the normalised capacity X is decreasing to zero, the term $C\,X/(D-X)$ in KiBaM model does not correctly describe the non-linear charge behaviour (overcharging) of the battery. It does not imply a strongly increased battery voltage at the end of the charging.
6) Improvements of the KiBaM model for overcharging could perhaps be possible by changing the variable X with D-X, in case of charging. Thus, the term $C\,X/(D-X)$, used in discharging, is replaced in charging by the term $C\,(D-X)/X$:

   $$E = E_0 + AX + C(D-X)/X \qquad \text{with } C > 0$$

   The decreasing of X to zero (in charging), would then imply a strongly increased battery voltage in overcharging.

It is also interesting to analyse if it is possible to describe both the non-linear charge behaviour (overcharging) and the non-linear discharge behaviour (over-discharging) by only one expression, as for example by:

$$E = E_0 + AX + \underbrace{\frac{C_1 X}{(D-X)}}_{\substack{\text{non-linear} \\ \text{discharge behaviour}}} + \underbrace{\frac{C_2 (D-X)}{X}}_{\substack{\text{non-linear} \\ \text{charge behaviour}}}$$

having the condition of negative parameter $C_1 < 0$ and positive parameter $C_2 > 0$. Parameter C_1 reflects the sharpness of end-of-discharge, while parameter C_2 indicates the sharpness of end-of-charge. Note that while the "non-linear" first term converges to infinite, due to a deep discharging, the second "non-linear" term converges to zero, and vice versa for an overcharging. In this way, both the extreme situations (overcharging and over-discharging) can be independently described.

It seems that this new voltage expression is one idea for a future detailed investigation of the battery modelling.

4.3 Controller

This section presents the background behind the modelling of the controller of a stand-alone PV system.

All power systems must include a control strategy that describes the interactions between its components. The use of battery as a storage form implies thus the presence of a charge controller.

The charge controller is used to manage the energy flow to PV system, batteries and loads by collecting information on the battery voltage and knowing the maximum and minimum values acceptable for the battery voltage. There are two main operating modes for the controller:

1) normal operating condition, when the battery voltage fluctuates between maximum and minimum voltages.
2) overcharge or over-discharge condition, which occur when the battery voltage reaches some critical values.

To protect the battery against an excessive charge, the PV arrays are disconnected from the system, when the terminal voltage increases above a certain threshold V_{max_off} and when the current required by the load is less than the current delivered by the PV arrays. PV arrays are connected again when the terminal voltage decreases below a certain value V_{max_on}. This can be done by using a switch with a hysteresis cycle, as illustrated in Figure 14.

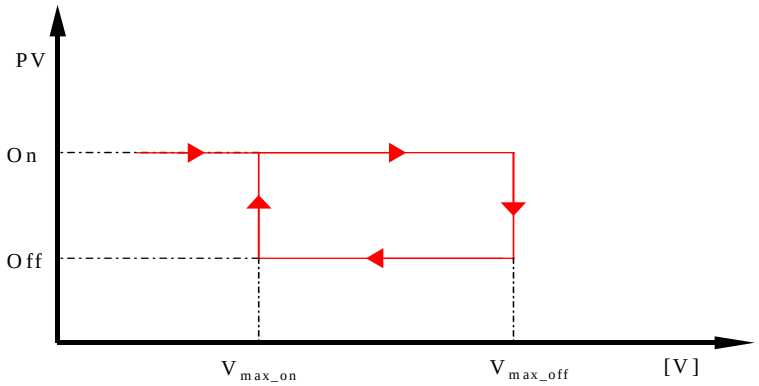

Figure 14: Operating principle of an overcharge protector.

To protect the battery against excessive discharge, the load is disconnected when the terminal voltage falls below a certain threshold V_{min_off} and when the current required by the load is bigger than the current delivered by the PV arrays. The load is reconnected to the system when the terminal voltage is above a certain value V_{min_on}, using a switch with a hysteresis cycle, as shown in Figure 15.

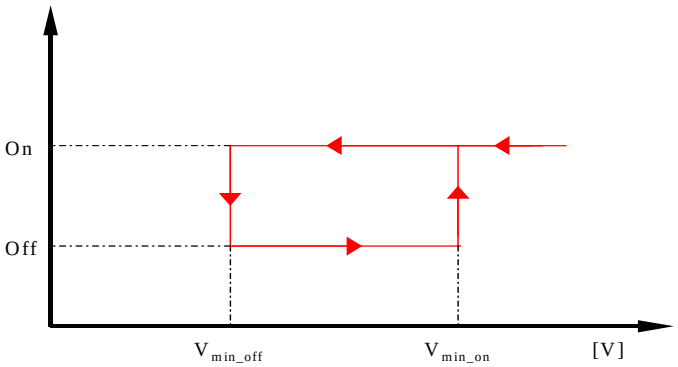

Figure 15: Operating principle of a discharge protector.

The switches may either be electromechanical (relay, contactors, etc.) or solid state (bipolar transistors, MOSFET's etc) – see (Lorenzo, 1994).

The steps in the modelling of the controller process are summarised in Table 3.

Table 3: Summary of the controller process.

	Constraint	***Command***
(1)	If $V>V_{max\_off}$ and $I_{load}<I_{pv}$	Disconnect PV arrays from the system
(2)	If command (1) is done and $V<V_{max\_on}$	Reconnect PV arrays to the system
(3)	If $V<V_{min\_off}$ and $I_{load}>I_{pv}$	Disconnect the load from the system
(4)	If command (3) is done and $V>V_{min\_on}$	Reconnect the load to the system

4.4 Load

The load existing in a PV stand-alone system can be of many types, both DC (television, lighting) and AC (electrical motors, heaters, etc.).

The PV stand-alone system at Risø contains an AC load, which is an electrical heater. This heater is actually a simple resistance controlled by a thermostat. Thus, the load can be modelled as:

$$I_{ac} = \frac{V_{ac}}{R_h}$$

where I_{ac}, V_{ac} are the AC-current and voltage of the load, respectively. R_h is the resistance of heater, which can be determined by the rated power P_{h_nom} and rated voltage V_{h_nom} of the heater, as follows:

$$R_h = \frac{\left(V_{h\_nom}\right)^2}{P_{h\_nom}}$$

4.5 Inverter

As known, the PV arrays produce DC power and therefore when the stand-alone PV system contains an AC load, as it is the case for the system at Risø, a DC/AC conversion is required. This is thus the reason why this section briefly presents the inverter.

An inverter is a converter where the power flow is from the DC to the AC side, namely having a DC voltage, as input, it produces a desired AC voltage, as output – see Figure 16.

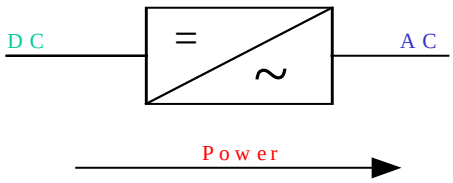

Figure 16: Connection of the inverter.

The inverter is characterised by a power dependent efficiency η. The role of the inverter is to keep on the AC side the voltage constant at the rated voltage 230V and to convert the input power P_{in} into the output power P_{out} with the best possible efficiency. The efficiency of the inverter is thus modelled as:

$$\eta = \frac{P_{out}}{P_{in}} = \frac{V_{ac}\ I_{ac}\ \cos\varphi}{V_{dc}\, I_{dc}} \qquad \Rightarrow \qquad I_{dc} = \frac{V_{ac}\ I_{ac}\ \cos\varphi}{\eta\, V_{dc}}$$

where I_{dc} is the current required by the inverter from the DC side (for example, from the controller) in order to be able to keep the rated voltage on the AC side (for example on the load). V_{dc} is the input voltage for the inverter delivered by the DC side, for example by the controller.

5 Implementation in Simulink

This section presents how the mathematical models of the components of a stand-alone PV system, described in Section 4, are implemented in Matlab/Simulink.

Simulink is a simulation program, which provides a graphical interface for building models as blocks diagrams. It offers the advantage of building hierarchical models, namely to have the possibility to view the system at different levels. Simulink provides also the possibility to build modular models, which have the advantage that in this way the models can be easily connected together in order to simulate a certain system (stand-alone or not stand-alone). Such models also help system designers to optimise the size of the components of the stand-alone PV system.

5.1 Models library

For practical use, the Simulink model blocks for each component of the stand-alone PV system can be gathered in a library. For example, the library can contain model blocks for a PV module, a battery, a load, an inverter and a controller – see Figure 17.

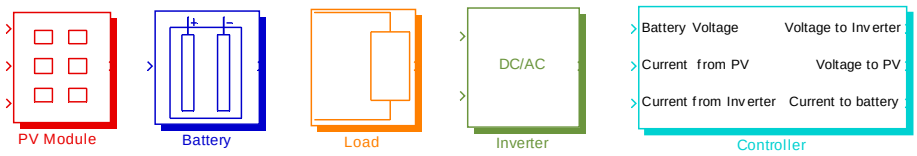

Figure 17: Simulink library for a PV stand-alone system.

The advantages of such a library are:

1) it gives a quick overview of which component models are available.
2) it is easy to just pick-up the components from the library, build a certain stand-alone PV system and simulate it.

An example of building a stand-alone PV system, by connecting directly the model blocks existing in the models library is illustrated in Figure 18. The total system has thus as inputs the irradiation and the ambient temperature. These are used in the PV module together with the voltage from the controller to generate the PV current. The controller achieves information from the battery, PV module and inverter. Based on these inputs and on the control dispatch summarised in Table 3, the controller transmits control signals back to the inverter, PV-module and battery. The DC voltage from the controller is thus applied to the inverter together with the AC current, which is required by the load. In order to be able to keep the rated voltage on the AC side to $V_{ac} = 230\,V$, the inverter requires further a specific value for DC current from the controller.

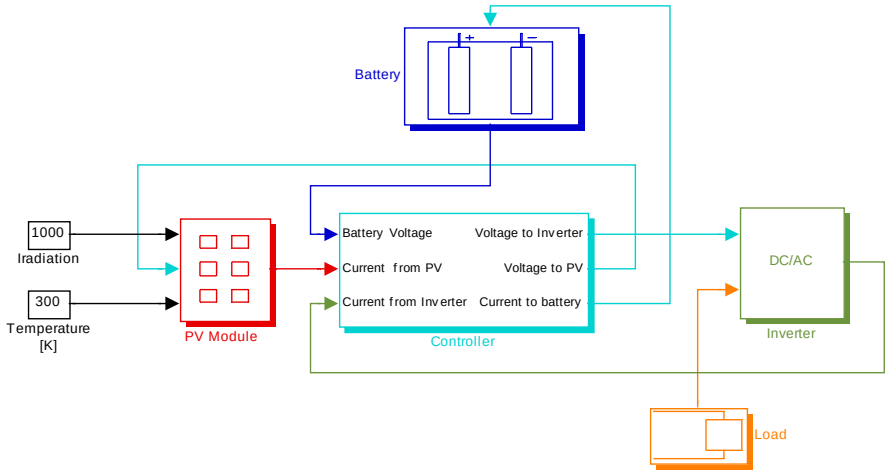

Figure 18: Stand-alone PV system structure in Simulink.

The basic blocks of the library can be used to built more specific structures, as for example an array structure, a battery bank structure. Figure 19 shows how the Solel PV array looks like. There are 3 three PV modules connected in parallel.

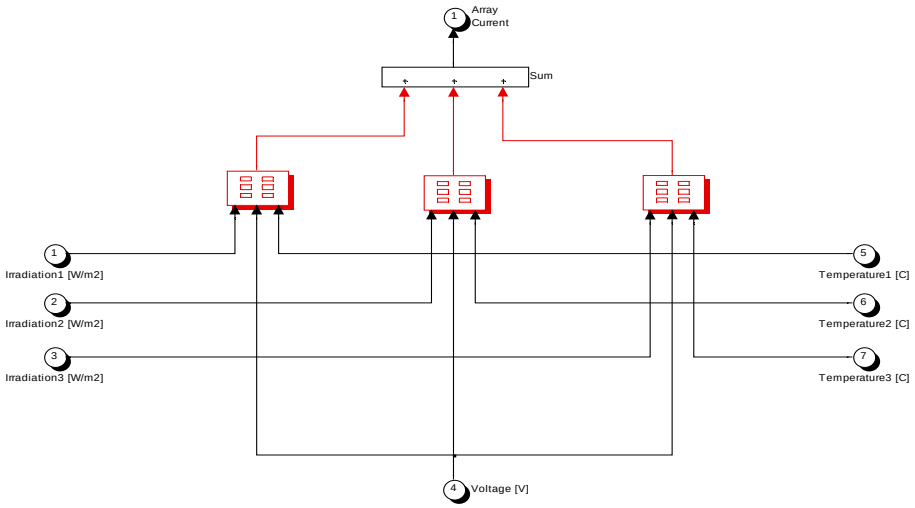

Figure 19 : Illustration of the Solel PV array structure.

Another powerful feature of the Simulink, called masking, is that it can simplify the use of the model by replacing many dialog boxes in a subsystem with a single dialog box. Instead of requiring the user of the model to open each block and enter parameter values, those parameter values can be entered on the mask dialog block and passed to the blocks in the masked subsystem. Figure 20, for example, illustrates how the mask dialog block for the PV module looks like. The user has just to change the values of the parameters for different types of PV modules, which eventually are used in the stand-alone PV system.

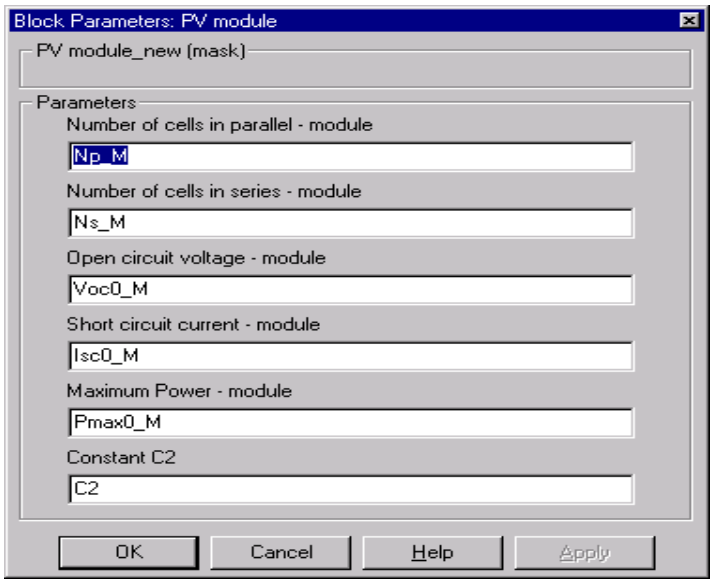

Figure 20: Mask parameters.

Masking makes it also possible to create a specific block icon that depicts the block's purpose – see Figure 17. Another advantage of masking is the prevention of unintended modification of subsystems by hiding their contents behind a customised interface.

5.2 Simulink model blocks

As mentioned, Simulink offers the advantage of buildings hierarchical models, namely to have the possibility to view the system at different levels. Thus each block can contain other blocks, other levels. For example, the internal "hidden" structure of the block "PV Module" from Figure 17, is illustrated in Figure 21. It represents the "detailed" Simulink implementation of the mathematical model of the PV module, describe in Section 4.1.2.

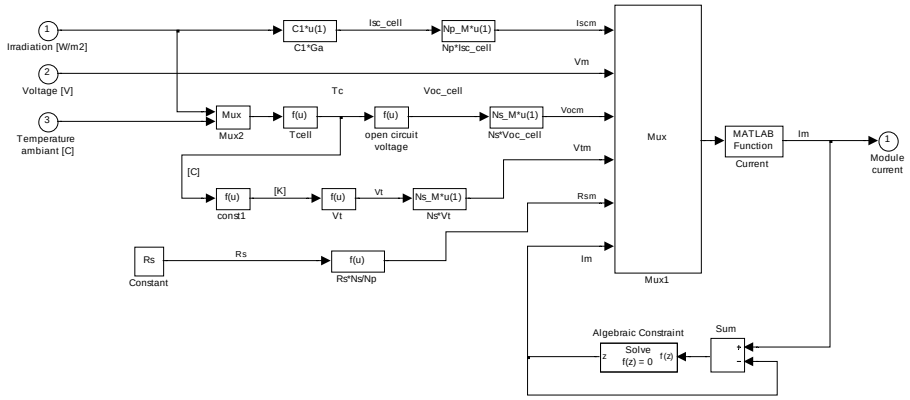

Figure 21: PV module structure.

The implicit function of the current I^M, for the PV module, as it was described in Section 4.1.2, can be solved easily by the "algebraic constraint" block, from Simulink (Version 5).

A brief overview of the internal structure of the others blocks of the Simulink library, presented in Figure 17, is provided in Figure 22, Figure 23, Figure 24, respectively. These figures contain the Simulink implementation of the mathematical models described in Section 4.

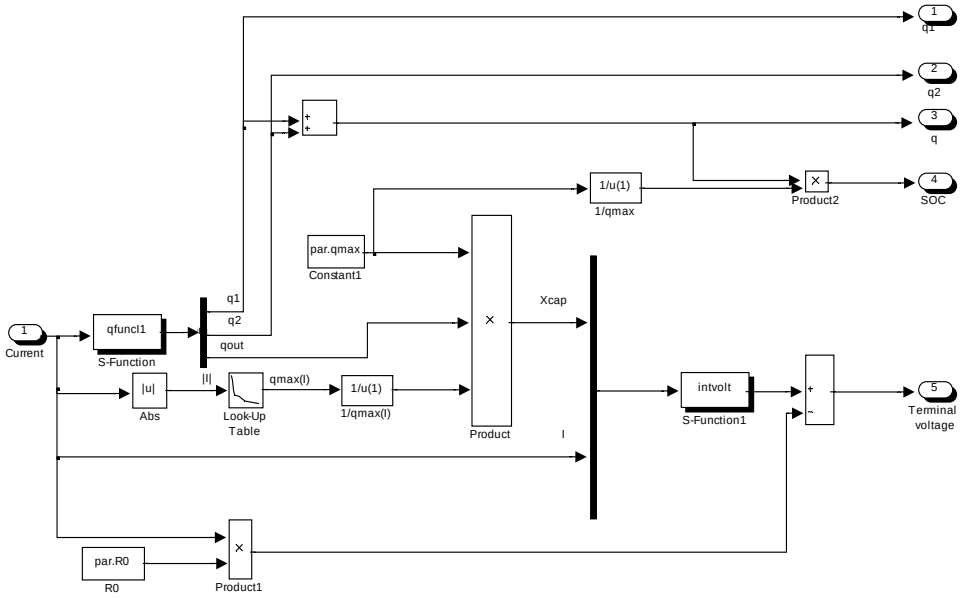

Figure 22: Simulink KiBaM battery model.

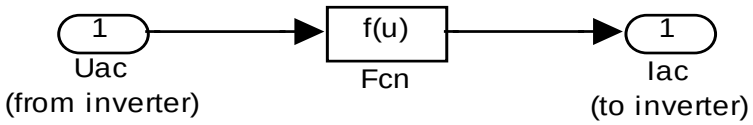

Figure 23: Simulink load model.

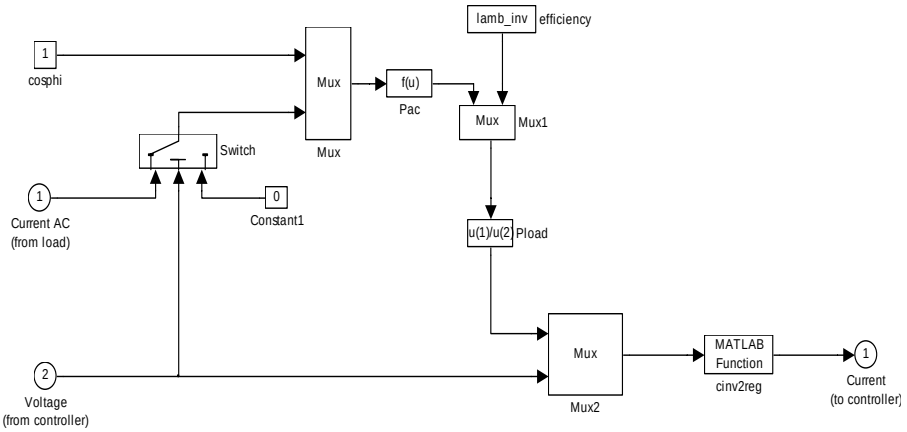

Figure 24: Simulink inverter model.

6 Measurement results and model validation

A set of measurements acquired from the stand-alone PV system at Risø, in the period from April 6th 2000 to April 22nd 2000, is used to validate the modelling of each component in the stand-alone PV system, presented in Section 4.

6.1 General on measurements

To facilitate the handling of data, the series of the measurements are divided into 4 periods:

- $set1data$ (period from April 7th 2000 to April 14th 2000)
- $set2data$ (period from April 14th 2000 to April 15th 2000)
- $set3data$ (period from April 15th 2000 to April 18th 2000)
- $set4data$ (period from April 20th 2000 to April 22nd 2000)

The time series of the irradiation, PV current, load current, battery current and battery voltage for all these 4 periods are presented in Appendix A.

Regarding the measurements, it is mentioned that:

- Only Solel arrays are coupled to the system during measurements. The Kyocera arrays are in open circuit and therefore the whole PV current is generated by the Solel arrays – see Figure 2.
- PV current is not measured. It is computed as $I_{pv} = I_{load} - I_{bat}$, according to Kirchhoff's current law, where I_{pv} is the PV generator current, I_{bat} is the battery current and I_{load} is the load current. Hence, the used convention is that the battery is seen as a generator, namely that in charging $I_{bat} < 0$ and in discharging $I_{bat} > 0$.
- In order to simplify the language, in the analysis of the measurements, the word "battery" will be used instead of "battery bank".

The quantities that are available in the measurements are presented in Table 4. In the analysis, both 1-minute average data and 1-second instantaneous time series data are available.

Table 4: Measured quantities.

G_a	Ambient irradiation	[W/m^2]
G_h	Horizontal irradiation	[W/m^2]
T_{amb}	Ambient temperature	[C]
V_{load}	DC voltage	[V]
V_{a5}	Kyocera array's voltage	[V]
V_{bat}	Battery voltage	[V]
I_{load}	DC current	[A]
I_{bat}	Battery current	[A]
V_{ac}	AC voltage	[V]
I_{ac}	AC current	[A]
P_{ac}	AC power	[W]
T_{bat}	Battery temperature	[C]
V_{a1}	Solel array's voltage	[V]

The most relevant parts of the series with particular events, from each of the four mentioned periods set of data, are chosen and analysed for understanding and modelling of the stand-alone PV system.

For example, in order to get a general idea about how the whole stand-alone PV system is working, such detailed sequence from *set2data* is picked-up and presented in Figure 25 and Figure 26. Focus is on April 15th 2000 from 10:00 to 18:00. In Figure 25, it can be seen that around 12 o'clock all 4 PV arrays are active, due to an intensive irradiation, no load and a battery voltage less than the critical overcharging value. The number of active arrays is not measured directly. It is estimated based on module's manufacturer data, on measured irradiation and measured PV current, as it is described in Section 6.2. The variations of PV current follow the variations of the irradiation.

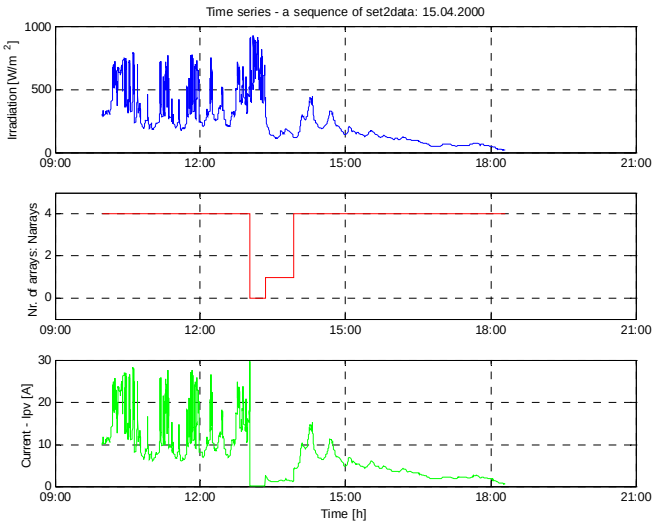

Figure 25: Irradiation G_a, no. of active PV arrays, PV current I_{pv} on April 15th 2000.

Figure 26 shows that around 12 o'clock, the load is not connected and the whole PV current is directly used in the charging of the battery. In the moment when battery voltage reaches the limit of the charging voltage $V_{\max\_off} = 27V$, the PV arrays are disconnected by the PV controller of the stand-alone PV system, in order to avoid overcharging. Thus PV current I_{pv} becomes zero for a period, see Figure 25. As there it is no load connected, the jump of PV current to zero is directly reflected to the battery current and further to the battery voltage – see Figure 26.

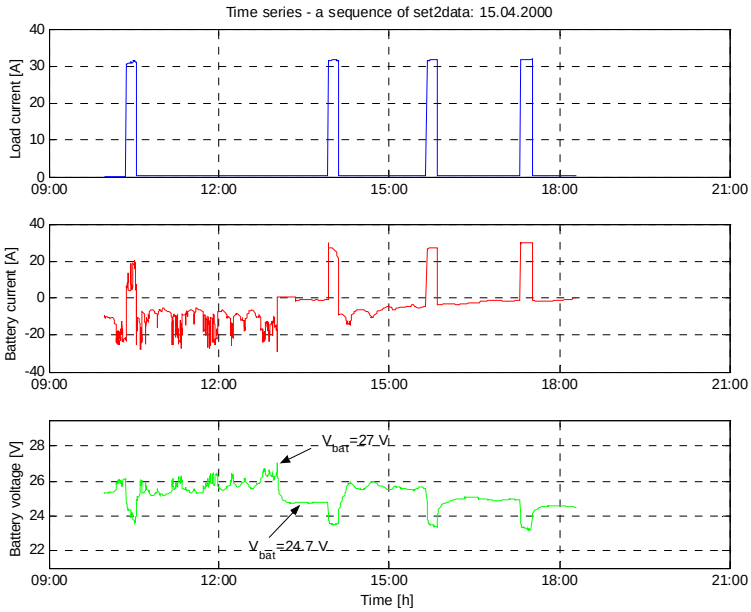

Figure 26: Load current I_{load}, battery current I_{bat} and voltage V_{bat} on April 15th 2000.

The battery is in a retrieving process (”retrieving after charging”) when $I_{PV} = 0A$ and $I_{load} = 0A$. It can be observed that the battery voltage is slowly decreasing. As it is illustrated in Section 6.3.3, in a retrieving process, the battery voltage follows almost an exponential function. In the moment when the battery voltage becomes 24.7V, one array is reconnected for a while. Shortly after, the load is connected, which causes all four PV arrays to be reconnected again. However, the PV current is not sufficient to supply the load and therefore current from battery is used. Thus, the battery is discharged as long as the load is connected. When the load is disconnected again, the battery voltage increases due to the surplus of PV current. It is observed that between 15:00 and 18:00, there are two other discharging periods, followed by retrieving periods (”retrieving after discharging”). It looks like that, after the last discharge, the state of charge of the battery is less than that from the beginning of the afternoon. It seems that it is difficult for the battery in the retrieving process to come back to the same voltage level.

In the following sections, an analysis of the measurements is performed and based on this, the models of each component of the stand-alone PV system, presented in Section 4, are validated.

6.2 PV model validation

The goal of this section is to validate the PV-model, described in Section 4.1.2. It is first shown how the model simulates the influence of irradiation and of cell temperature on the PV module's efficiency. Then, there is a comparison between measurements and simulations of the PV-model, simulations that are performed with real data from measurements.

The Simulink implementation of the PV module, illustrated in Figure 21, is used to perform a simulation of the PV module for different values of irradiation and cell temperature – see Figure 27. The first subplot in Figure 27 illustrates how the I-V curve of the PV module is affected by irradiation, when the cell temperature is kept constant to $T_c = 25\ ^\circ C$. The second subplot shows the influence of the cell temperature on I-V curve, when the irradiation is kept constant to G_a=1000 W/m^2.

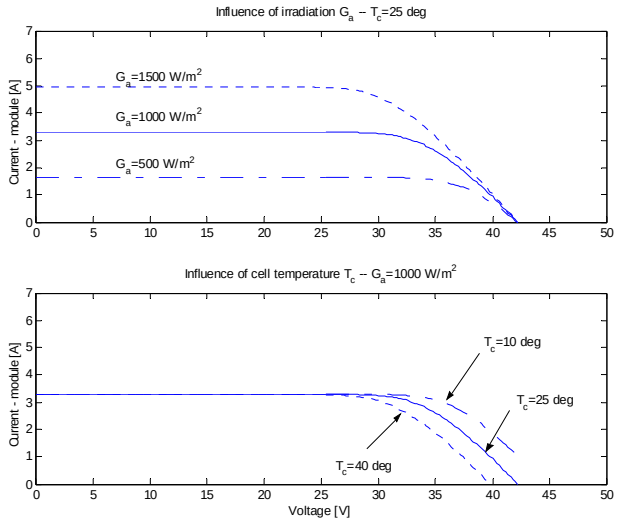

Figure 27: Influence of irradiation G_a and of cell temperature T_c.

It is observed that the short circuit current of the PV module depends exclusively and linearly on the irradiation ($I_{sc} = C_1 G_a$), while the open-circuit voltage V_{OC} increases logarithmically with the irradiation. The dominant effect of the increased cell temperature is the decrease of open-circuit voltage V_{OC}.

In Figure 28, it is for example illustrated the period of time April 7th 2000 to April 14th 2000, where the ambient temperature fluctuates up to $15^\circ C$ and irradiation up to $1200\ \text{W/m}^2$. As mentioned in Section 4.1.2, the cell temperature T_{cell} can be approximated as $T_{cell} = T_{amb} + 0.03 \cdot G_a$. Thus, even for the gentle conditions existing in the mentioned period, the cell temperature can come up to $50^\circ C$.

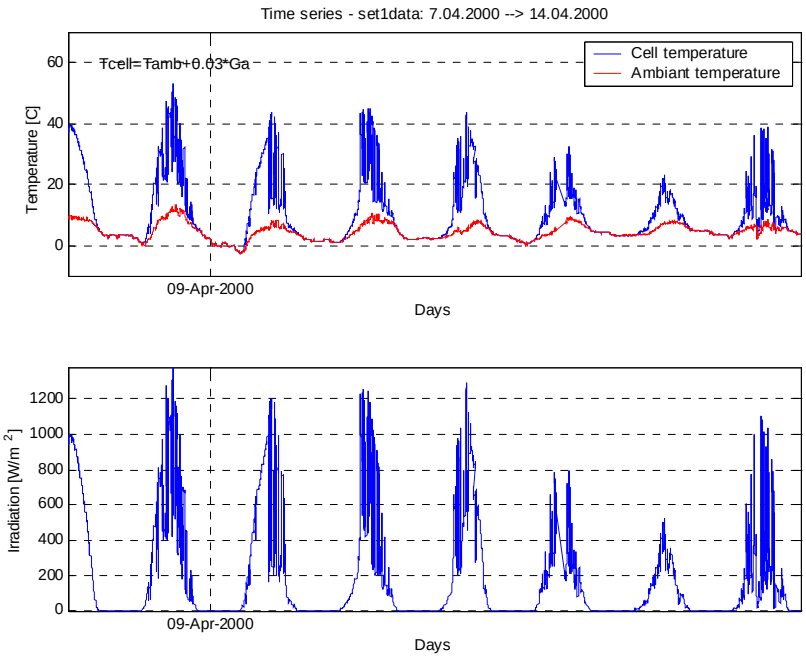

Figure 28: Ambient temperature T_{amb}, cell temperature T_{cell} and irradiation G_a in case of set1data.

For the same period, it is interesting to look on the PV current, number of active arrays and battery voltage - see Figure 29. In this period, described by *set1data*, the load is not connected – Appendix A. Therefore, the whole PV current is used to charge the battery. Thus, variations of the PV current are seen further as variations in the battery voltage.

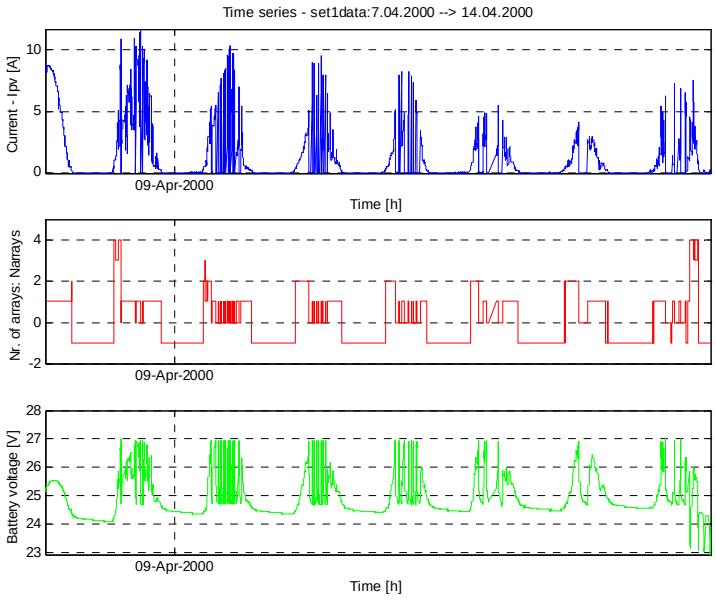

Figure 29: PV current I_{pv}, number of active PV arrays and battery voltage V_{bat} in case of set1data.

The PV arrays are connected or disconnected by the PV controller, which uses information about battery voltage, PV current and load current – see Section 4.3. In order to get an idea about the efficiency of the PV system, it is necessary to know at each moment how many PV arrays are connected to the system. The information about the number of connected arrays can also be used in the simulation of the system. The number of connected PV arrays can be estimated using the relation:

$$N_{arrays} = round\left(\frac{I_{pv}}{G_a} \cdot \frac{1000}{35/4}\right)$$

where function "$round(x)$" rounds x to the nearest integer. This approximation is based on two assumptions: 1) PV current is proportional to the ambient irradiation 2) The manufacture's data for Solel module attest that, in standard conditions ($G_a = 1000\,W/m^2$ and $T_{cell} = 25^{\circ}C$), the short circuit current and the open-circuit voltage of the Solel module are: $I_{sc} = 3.31\,A$ and $V_{oc} = 42.2\,V$ (see Appendix B). This means that for an operating point around $V_{bat} = 24\,V$ one module produces around 3A, while an array with 3 modules produces close to 9A ($round(35/4) = 9$).

As illustrated in Figure 2, the PV system contains 4 Solel arrays. Therefore, the number of active arrays can vary between 0 and 4. The value "-1", observed in Figure 29, is intentionally inserted in order to denote the situations with possible numerical problems in the estimation of N_{arrays}. For example, during nights the irradiation is zero and this implies a division by zero in the computation of N_{arrays}.

A comparison between the measurements and the simulations of the PV arrays is performed. Figure 30 shows the Simulink scheme for the four coupled in parallel Solel PV arrays – see Figure 2. Each Solel array has the structure presented in Figure 19. Inputs in the scheme are the measurements on irradiation, battery voltage and ambient temperature, from $set1data$. In order to make the simulation strategy as close as possible to the measurements, the previous computed number of connected arrays N_{arrays} is used as input to a virtual PV controller. This virtual controller is implemented to simulate the consecutive connection of each array (from array (1) to array (4)) or disconnection of each array (from array (4) to array (1)). The intermediate information N_{arrays} is used in the virtual controller, due to the insufficient knowledge on the actual internal dispatch strategy of the analysed stand-alone PV system. The output of the scheme is the simulated current from four arrays.

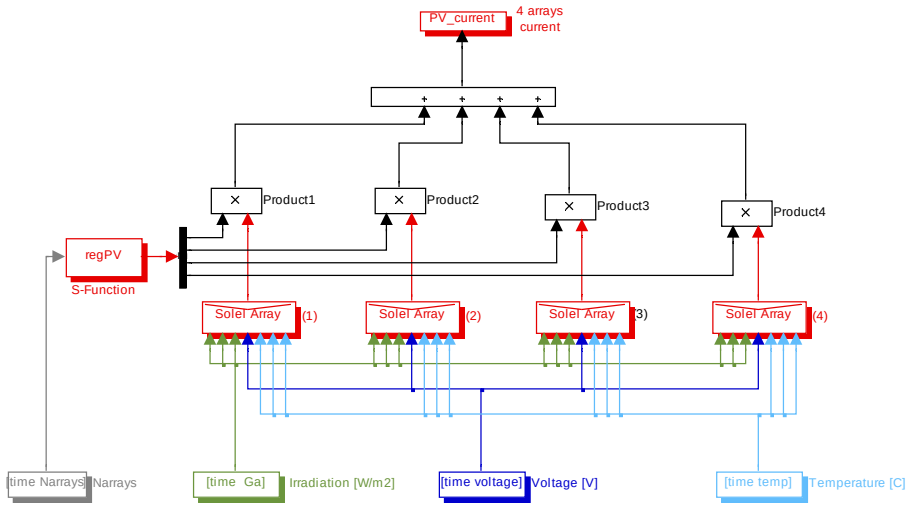

Figure 30: Simulink model for four PV arrays and one PV controller.

In Figure 31, the simulated and the measured current from the four PV arrays versus ambient irradiation are plotted. Each inclined ramp in the figure, both for measurements and for simulation, corresponds to a certain number of connected PV arrays. For example, the ramp with the lowest gradient, different from zero, is equivalent to the situation when only one array (the first) is connected. The ramp with twice the gradient of the first ramp corresponds to the situation with two PV arrays active, and so on.

In the measurements, it is observed that there exist three dominant situations, namely 1) when only the first array is coupled, 2) when the first two arrays are connected and 3) when all four arrays are coupled to the system. The case with three connected arrays is switched quickly to the situation with four connected arrays. Notice that in the simulation there are four distinctive ramps. The reason for this is that, in the simulation it is used the estimated number of the connected arrays N_{arrays}, based on the efficiency of the PV system determined from manufacture's data and not based on measurements.

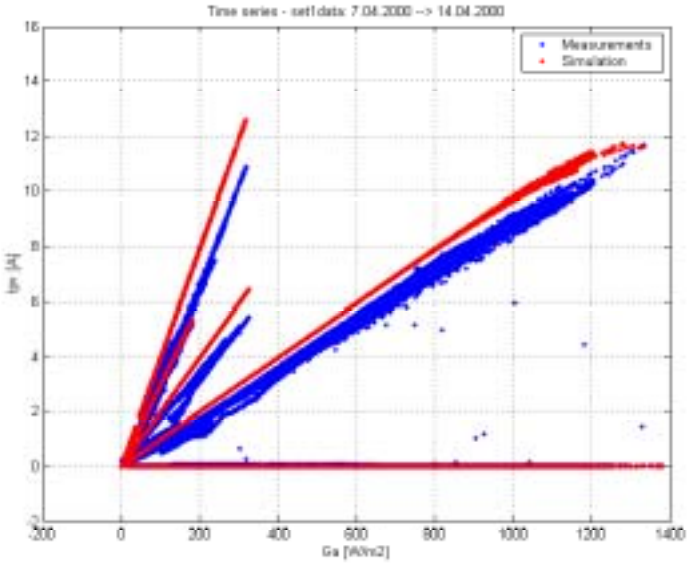

Figure 31: PV current I_{pv} versus irradiation G_a : measurements (set1data) and simulation.

It is noticed that the measured current is lower than the simulated current. It seems that the measured efficiency of the PV system is almost 15% less than the simulated efficiency. There are possible reasons for this:

- Measurements are acquired in realistic weather conditions, i.e. with panels subjected to dust etc.
- The simulation of the module is performed based on the rated data of the PV module, (supplied by the manufacture) and not on the specific measured data for the module.
- PV model's uncertainty.
- Measurements' uncertainty.
- Ageing of the cells.
- The cell temperature is approximated and not measured directly.

Figure 31 also illustrates an interesting phenomenon, which appears in the measurements at low irradiation, namely a number of measurements forms a deviated track shape from the expected linear correlation. As this deviation appears when the irradiation level is low, it can be interpreted as being due to dewdrops on the panels early in the morning or due to shadows in the afternoons.

Another interesting phenomenon appears at high irradiation levels (over 1000 W/m^2). Here the simulated current exhibits a bending shape, which seems to become more spread towards the end. In order to understand this phenomenon related with the simulated current, a specific set of 6 cases are simulated for the PV module (see Figure 21): ambient temperature is kept consecutively constant to two values ($0^\circ C$ and $15^\circ C$), the voltage is kept consecutively constant to three values (21V, 24V and 27V), while the irradiation is varying linearly from 0 W/m^2 to 1500 W/m^2. These values for voltage and ambient temperature in the simulation are chosen to include the whole range of measurements from $set1data$. Figure 28 shows that the ambient temperature varies between $0^\circ C$ and $15^\circ C$, while Figure 29 shows that the voltage varies between 24V and 27V. Figure 32 contains the simulation results for these 6 cases.

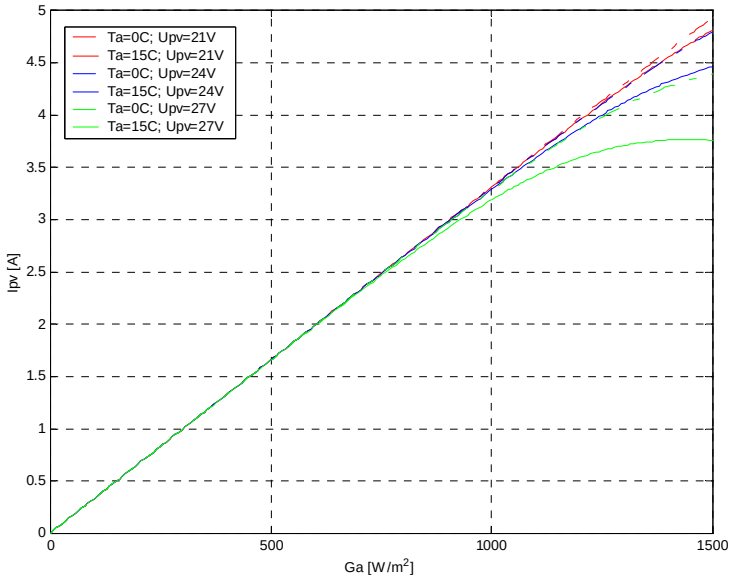

Figure 32: Influence of cell's temperature and voltage on the PV current at high irradiation levels.

Again, it is observed that a bending shape in the linear curve appears at high irradiation levels, depending on how high both the ambient temperature and applied voltage are. It seems that, due to the empirical used relation $T_{cell} = T_{amb} + 0.03 \cdot G_a$, the simulated cell temperature increases rapidly at high irradiation levels and the ambient temperature becomes thus an important parameter. However, one should have in mind that the relation $T_{cell} = T_{amb} + 0.03 \cdot G_a$ is an approximation, and therefore it does not necessary reflect correctly the reality. Perhaps, the real cell temperature is not so high as it is simulated.

In Figure 27, it was illustrated that an increased cell temperature makes the PV module less efficient. The I-V curve is moving to the left with a higher T_{cell} (see Figure 27) and thus the PV module's characteristic becomes poorer for the same high operating voltage. If, in these conditions, the operating voltage increases, the performance of the PV modules decreases even more. Hence, the higher voltage applied to the PV array is, the bigger the influence of the ambient temperature is on the bending of the curve $I_{pv} = func(G_a)$. For example, in Figure 32, the band limited by the curves $(T_a = 0^\circ C,\ V = 27\,V)$ and $(T_a = 15^\circ C,\ V = 27\,V)$ is wider than the band limited by the curves $(T_a = 0^\circ C,\ V = 24\,V)$ and $(T_a = 15^\circ C,\ V = 24\,V)$. This is also reflected by the spreading of the bending towards high irradiation for the simulated current - see Figure 31. As this phenomenon does not appear in the measurements, further investigation of the PV model is needed for the operation conditions: high irradiation, high ambient temperature and high operating voltage.

The following summarises a number of final observations:

- The simulated efficiency of the PV module is higher than the measured efficiency of the PV module.
- The description of the cell temperature is probably not accurate. A measurement of the cell temperature could improve the simulation of the PV module.
- The model of PV module should be used cautiously in the case of high irradiation, high ambient temperature and high operating voltage.

6.3 Battery model validation

This section focuses on the analysis and understanding of the battery's behaviour, and on comparison between the measurements and the simulation results of the KiBaM model – described in Section 4.2.2.

6.3.1 General overview on the battery's behaviour

First, in order to illustrate how the PV system (with focus on the battery) works, the sequence of measurements performed on the afternoon of April 16th 2000 (from $set3data$), is considered – see Figure 33 and Figure 34. It is observed that between 12 o'clock and 14:30 all four PV arrays are connected, due to an intensive irradiation and a non-too-high battery voltage. The battery is charged over two hours. Around 14:00, the load (electrical heater) is connected for a while by the thermostat, which makes the battery enter the discharging mode. When the load is disconnected, the battery is again in the charge regime. It seems that close to 14:30, the battery voltage reaches the charging limit of 27V,

and therefore all four PV arrays are disconnected for a while by the PV controller of the system. However, shortly after the first array is reconnected and later on the second one – see Figure 33. As irradiation at this moment is not high and still decreasing, the current produced by these two active arrays is limited. Therefore, around 17:00, when the load is connected by the thermostat - Figure 33, the PV controller of the system activates all four PV arrays.

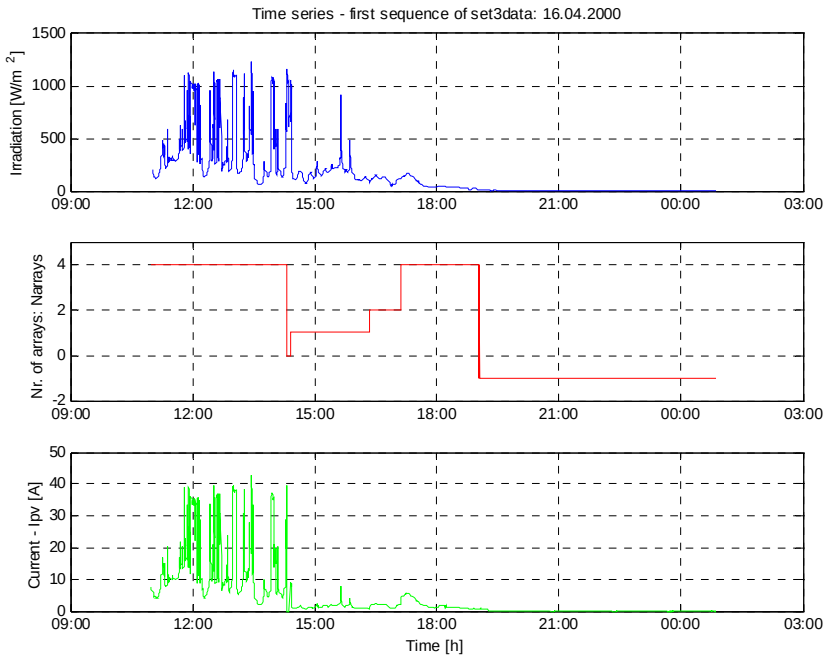

Figure 33: Irradiation G_a, number of active PV arrays, PV current I_{pv} for April 16th 2000, from 12 o'clock to midnight.

Since the irradiation level is close to zero late in the afternoon, each coupling of the load now implies a progressive discharging of the battery.

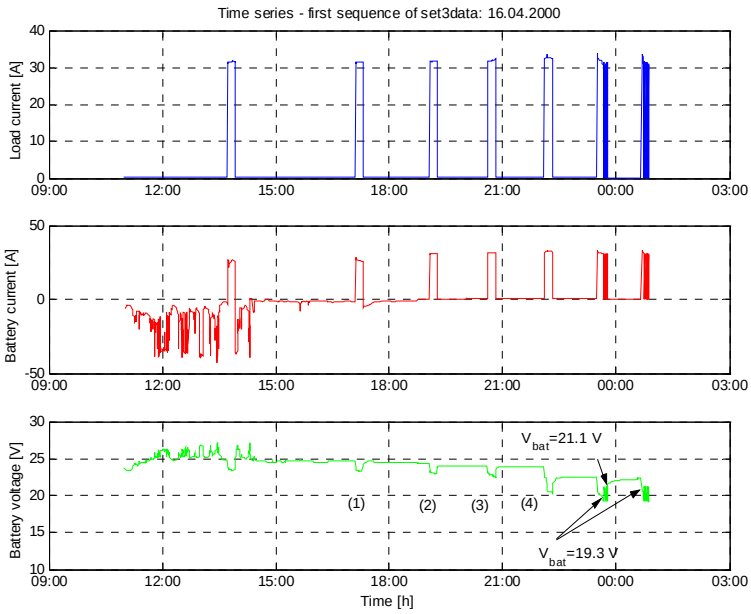

Figure 34: Load current I_{load}, battery current I_{bat} and voltage V_{bat} for April 16th 2000, from 12 o'clock to midnight. The numbers (1) to (4) in the battery voltage subplot, indicate sequences, which are further discussed in Figure 35.

In Figure 34, the four consecutive discharge regimes after 15:00 are numbered from (1) to (4), in order to be presented in more details in Figure 35.

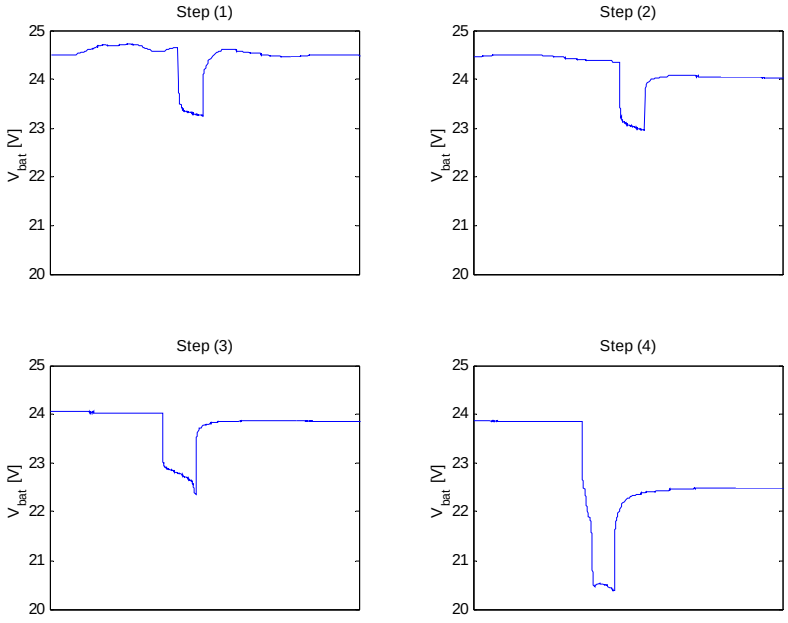

Figure 35: Focus on the battery voltage performance for the four discharge regimes, numbered as (1), (2), (3), (4) in Figure 34.

It is seen in Figure 35 that the voltage level in discharging continues to decrease, as the number of the discharge regimes is increased. The figure clearly displays the non-linear behaviour of the battery. The form of the discharging curve is changed, as the discharge regimes are progressed. The battery benefits

from the load being disconnected by the thermostat, after short periods. This gives the battery the possibility to go through a retrieving process, after each discharging. It is also observed that the voltage level after the retrieving process is lower (from ca. 24.5 V for step (1) to ca. 22.5 V at step (4)), this being a sign that the battery's state of charge **SOC** is decreased. The term state of charge **SOC** gives an indication of the depth to which the battery is charged. It seems that during discharging number (3), the battery is very close to be fully discharged, this being indicated by the deep and sharp voltage drop at the end of the discharge period. It is fortunate that at this moment the load is disconnected by the thermostat. However, the consistent discharging of the battery results in a deeper and quicker running down of the voltage – see discharging (4).

Figure 34 illustrates that around midnight the battery voltage reaches the critical low value for the inverter $V_{\min\_off}^{inv} = 19.3V$. At this value, the inverter controller disconnects the load, due to the low value of the DC voltage. It is noticed that when the battery voltage comes up to $V_{\min\_on}^{inv} = 21.1V$, the inverter controller reconnects the load – see Section 6.5. Since the battery voltage is close to the critical discharge value, and thus the voltage on the DC side of the inverter is too low, the load is switched "on" and "off" by the inverter controller a number of times, until the thermostat disconnects the load due to a high room temperature. This action is independent of the value of the battery voltage, determined by the ambient/room temperature and irradiation. As expected, the coupling period of the load (electrical heater) is larger during the night – see Figure 34. However, the coupling period is in average about 12-15 minutes.

6.3.2 Estimation of the internal resistance of the battery

Based on the measurements presented in Figure 33 and Figure 34, an estimation of the internal resistance R_0 of the battery is performed.

The assumption behind the estimation method of R_0 is that the state of charge **SOC** of the battery is the same just before and just after a step change in the battery current I_{bat}. Thus, it is assumed that the change in the terminal voltage V_{bat} is only caused by the change in the voltage drop over the internal resistance. As described in Section 4.2.2, the terminal voltage of the battery is given by:

$$V_{bat} = E - I_{bat} \cdot R_0$$

where: E = internal battery voltage, which varies with the state of charge **SOC**
V_{bat} = battery voltage (alias terminal voltage of the battery)
I_{bat} = battery current
R_0 = battery internal resistance

As the internal voltage E is assumed to be a function only of the state of charge **SOC**, the instantaneous steps in current affects the terminal voltage V_{bat} through the term $I_{bat} \cdot R_0$. Thus, the internal resistance can be estimated by:

$$R_0 = \frac{\Delta V_{bat}}{\Delta I_{bat}}$$

where ΔV_{bat} and ΔI_{bat} are the steps in terminal voltage and battery current, respectively. For example, Figure 36 presents a zoom of a single step in current

and voltage (the first in the period from 18:00 to 21:00). The measurement points are indicated by the sign "x". By computing ΔV_{bat} and ΔI_{bat} for all such similar steps in voltage and current, respectively, the variation in time of the internal resistance R_0 can be determined.

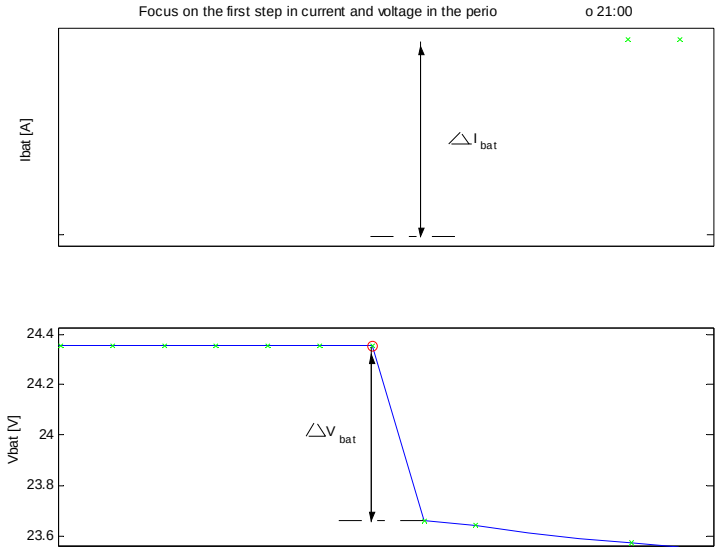

Figure 36: Current and voltage steps adequate for computation of the internal resistance R_0.

Figure 37 illustrates the steps (positive and negative - marked by circles) in the battery current and voltage, which are used in the estimation of the internal resistance R_0. For each such step (before connection of the load and after disconnection of the load) the internal resistance is estimated. Between steps, the value of R_0 is assumed to be constant to its last value.

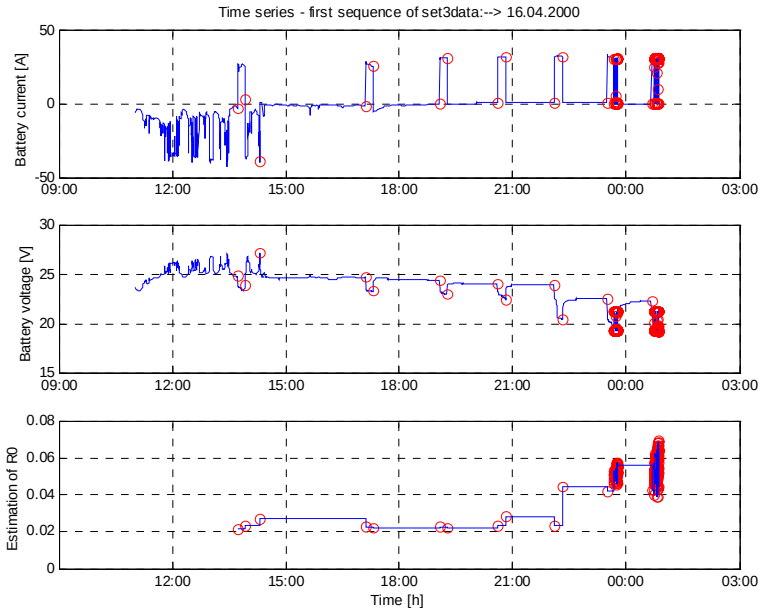

Figure 37: Estimation of the internal resistance R_0.

The third subplot of Figure 37 shows the estimated value of R_0 over time. It looks like that, before 15:00, the battery is charged with a large current (around 40A) and that the internal resistance is increased. However, this is not very reliable from a numerical point of view, due to the existing spikes in the current in this period. Further, it is observed that as long as the battery state of charge **SOC** is high, i.e. the battery voltage is high and almost constant, the internal resistance of the battery is constant during discharging (see behaviour between 17:00 and 21:00). However, after several periods of discharging, the battery state of charge **SOC** is not so high anymore and therefore the battery voltage falls deeper and more quickly. It is observed that the internal resistance increases during deep discharging (see behaviour between 21:00 and midnight). As it was described in the previous section, close to the midnight the load is switched ”on” and ”off” by the inverter controller, due to the low value of the DC voltage, this being also visualised in Figure 37. This period is again not reliable in the estimation of the internal resistance.

There is a general tendency for the estimated values of the internal resistance R_0, to return to the same level of $0.022\,\Omega$. This observation could be a reason to consider the internal resistance R_0 constant in time i.e. equal to $0.022\,\Omega$.

The idea of the following analysis is to see whether or not the instantaneous fluctuations in the terminal voltage V_{bat} also appear in the internal voltage *E*.
In this investigation, a sequence from $set2data$ with focus on April 15th 2000, where only charging occurs, is considered.

Figure 38 illustrates this charging sequence. The third subplot shows the removed capacity q_{out} over the charging regime, as being the integral of the battery current $q_{out} = \int I_{bat}\, dt$. As expected, during a continuous charging the removed capacity is numerically increasing in absolute value. The negative sign is due to the used sign convention, namely $I_{bat} < 0$ during charging. As the considered charging sequence is picked up from $set2data$ just between two discharging regimes, the removed capacity is set to zero at the beginning of charging.

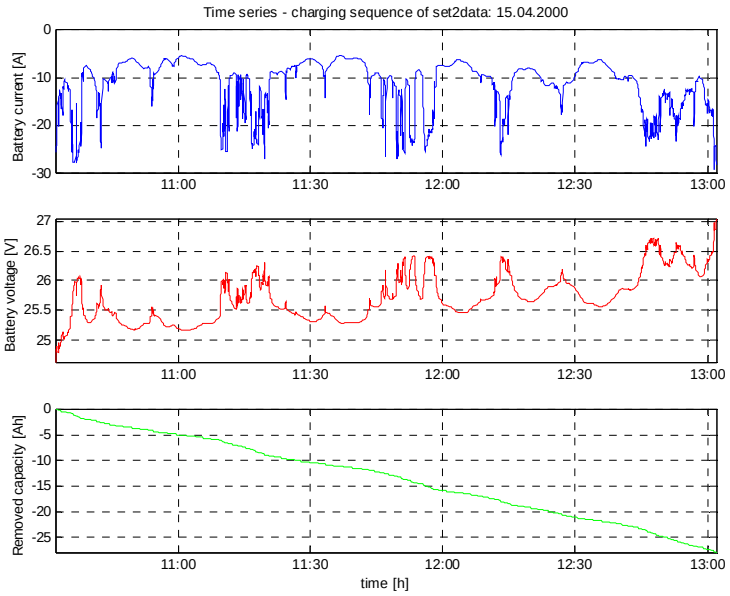

Figure 38: Charging sequence: battery current I_{bat} *, terminal battery voltage* V_{bat} *and removed capacity* q_{out} *.*

Figure 39 illustrates both the terminal voltage V_{bat} and the internal voltage E versus removed capacity q_{out}, for the charging sequence of $set2data$ presented in Figure 38. The internal voltage is computed with the relation $E = V_{bat} + I_{bat} \cdot R_0$, where the estimated internal resistance $R_0 = 0.022\,\Omega$ has been used. It is observed that, while the slow variation of the internal voltage E is similar to the slow variation of the terminal voltage V_{bat}, the rapid fluctuations in the terminal voltage V_{bat} are not anymore present in the internal voltage E. As it was assumed in the estimation of the internal resistance R_0, it seems that the difference term $I_{bat} \cdot R_0$ is the cause of the rapid fluctuations (instantaneous variations) in the terminal voltage *V*. The slow variation existing in the internal voltage E is an expression of its strong dependency on the state of charge **SOC** of the battery**.** It indicates that the dynamics of the battery are highly non-linear.

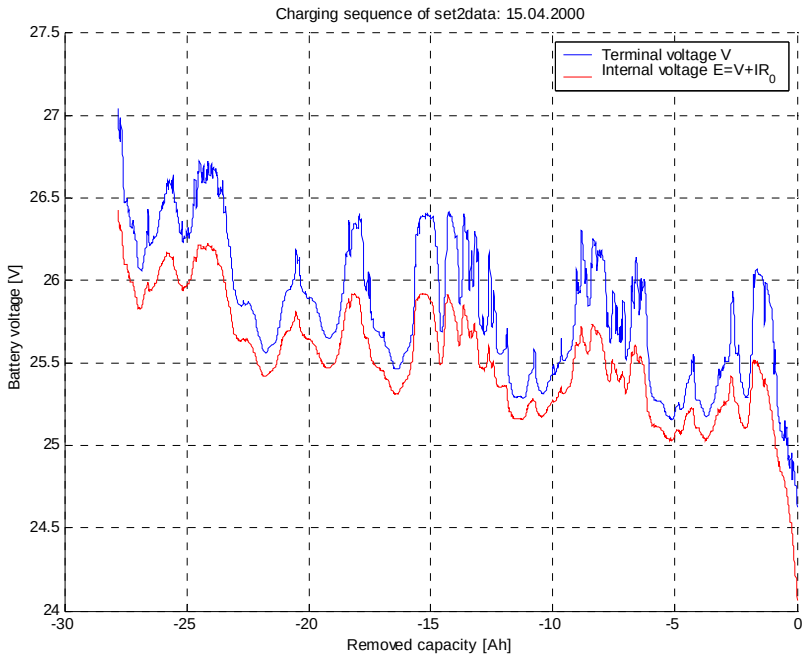

Figure 39: Battery voltage V_{bat} versus removed capacity q_{out}.

Thus, it can be concluded that:

- the simple model $E=V_{bat} - I_{bat} R_0$ does not present a sufficient modelling of the internal voltage of the battery E.
- the internal voltage of the battery E is strongly dependent on the discharge/charge current and on the state of charge **SOC** of the battery.
- the presented estimation method of R_0 has some limits from a numerical point of view. However, it seems that the internal resistance has the tendency to increase when the battery is strongly discharged.

6.3.3 Estimation of parameters for the retrieving process

The mode of operation where the battery current is zero, is called the retrieving process. It reflects the "idle" behaviour of the battery during a rest process, when the battery voltage gets back to a stationary state of equilibrium. Two types of retrieving are considered:

1. "retrieving after charging" - when the voltage slowly decreases to a stationary state of equilibrium, after a charging process.
2. "retrieving after discharging" - when the voltage slowly increases to a stationary state of equilibrium, after a discharging process.

Figure 40 illustrates an example of "retrieving after charging", in the sequence picked from *set2data* and presented in Figure 26.

When the battery current is zero, it is fair to assume $E=V_{bat}$. Furthermore, the response in the voltage after charging or discharging presents information on the internal dynamics of the battery. Hence, assuming this dynamic behaviour to be described as a first order system, the voltage response can be modelled by an exponential function in time domain:

$$\hat{V}_{bat} = a + b \cdot \exp(-c \cdot t)$$

where a, b and c are the parameters which characterise the time response. For the case illustrated in Figure 38, the parameters have been estimated to $a = 24.73$, $b = 1.28$ and $c = 0.0056$. The time constant is estimated to $\tau = \frac{1}{c} = 179$ seconds. The estimated voltage is also shown in Figure 40, i.e. the simulated response using the estimated parameters. It is seen that the exponential function fits the measurements well.

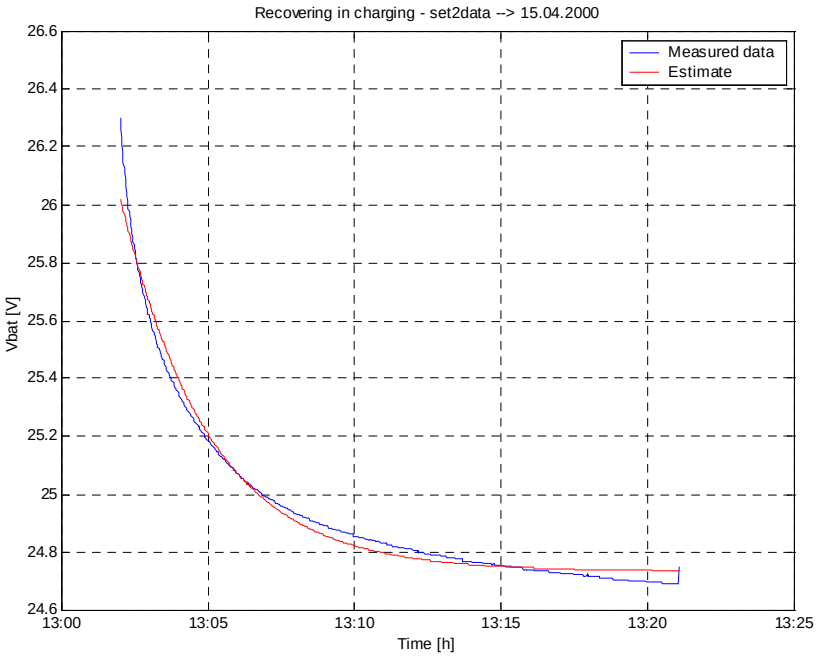

Figure 40: Example of "retrieving after charging".

Similar estimations are also performed for other similar retrieving periods. Estimation results for these are presented in Table 5.

Table 5: Estimated voltage model's parameters in retrieving mode.

a	**b**	**c**	**τ [s]**	**Date**	**Type of retrieving**
24.73	1.28	0.0056	179	15.04.2000	Retrieving after charging
24.05	-0.30	0.0093	108	16.04.2000	Retrieving after discharging
23.86	-0.35	0.0078	128	16.04.2000	Retrieving after discharging
22.48	-0.78	0.0037	270	16.04.2000	Retrieving after discharging
24.73	1.07	0.0015	667	22.04.2000	Retrieving after charging

Parameter a indicates the final voltage level in the retrieving process, b reflects an amplification (amplitude) of the exponential function, while c is a measure of the time constant τ of the assumed first order behaviour.

It is noticed that the time constant τ in retrieving process after charge is not equal to the time constant τ in retrieving after discharge. It seems that, the time constant τ in retrieving is strongly dependent on the battery state of charge **SOC.** This fact is clearly visualised especially by the estimation of the parame-

ters in all three retrieving after discharging (2), (3) and (4), existing on April 16th 2000 – see Figure 34. It is observed that the time constant τ in retrieving increases after the battery is consistently discharged. The battery state of charge **SOC** becomes lower and it takes more time for the battery to reach a stationary state of equilibrium.

6.3.4 Illustration of the highly non-linear dynamic of the battery

The purpose of this section is to illustrate by measurements the highly non-linear behaviour of the battery.

A detailed sequence, which illustrates the dynamics of the battery, is presented in Figure 41 and Figure 42. Focus is on April 17th 2000 between 6:00 and 18:00.

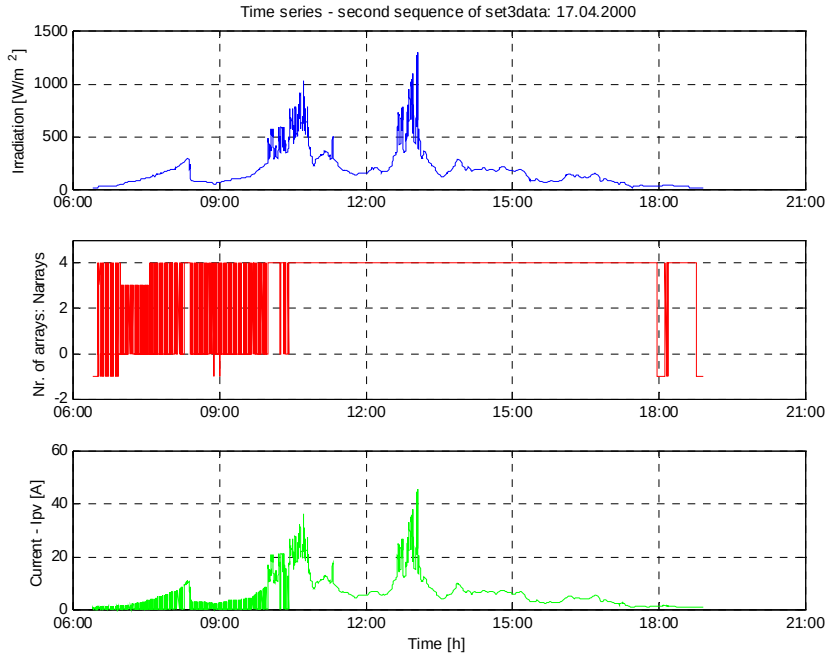

Figure 41: Irradiation G_a, number of active PV arrays, PV current I_{pv} on April 17th 2000.

It can be observed that all night long until 10 o'clock in the morning (see Appendix A) the load is switched "on" and "off" by the inverter controller, since the battery is completely empty after the progressive discharging. The battery voltage falls down to $17\,V$, a value which is much lower than the low voltage value of the inverter $V_{\min\_off}^{inv} = 19.3\,V$. The irradiation level starts to increase early in the morning and all PV arrays are connected. However, the PV current I_{pv} continues to be smaller than the load current I_{load} and thus the battery continues to be discharged. The battery state of charge **SOC** persists to be very low. Finally, around 10:30 in the morning, the irradiation is strong, the load is disconnected and the battery is charged.

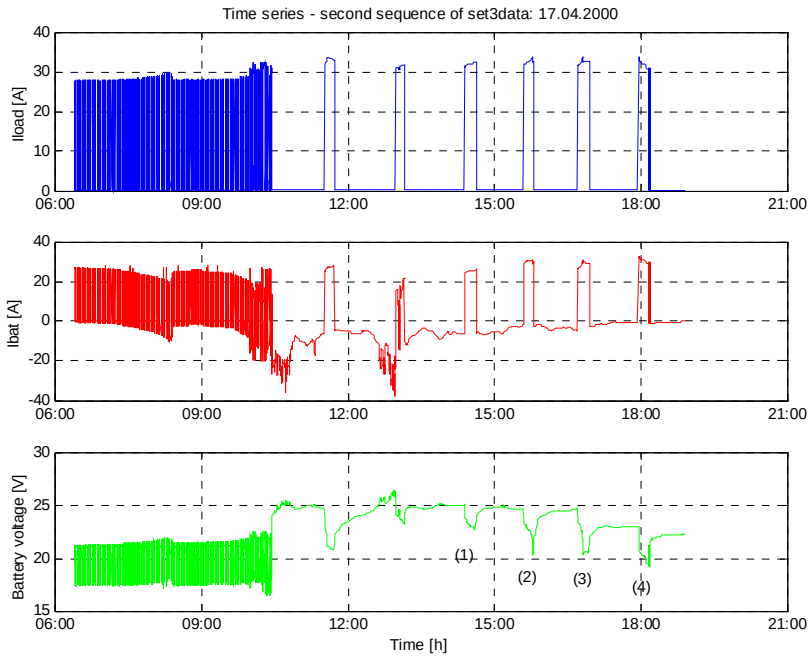

Figure 42: Load current I_{load}, battery current I_{bat} and voltage V_{bat} on April 17th 2000. The numbers (1) to (4) in the battery voltage subplot indicate sequences, which are further discussed in Figure 43.

An indication of the highly non-linear dynamics of the battery is the discharging behaviour between 14:00 and 18:00. In Figure 42 the four consecutive discharge regimes after 14:00 are numbered from (1) to (4), in order to be presented in more details in Figure 43.

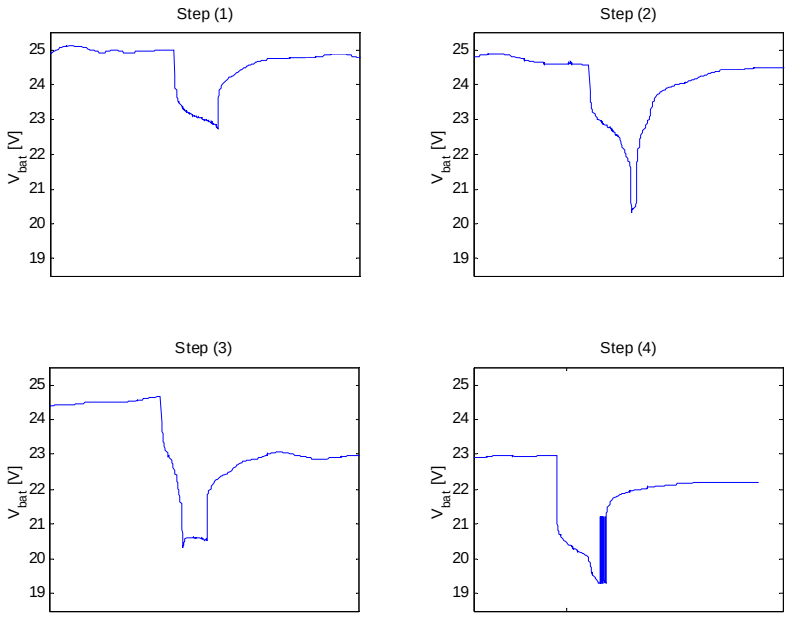

Figure 43: Focus on the voltage for four discharge regimes, numbered as (1), (2), (3), (4).

It seems that after a whole night with switching "on" and "off", the state of charge **SOC** of the battery is very low. The battery voltage falls deeper during the persistent discharge regimes. The voltage is again close to collapse, however this time following a more complex curve. On the way down, it seems that the battery voltage reaches a "corner" level (see discharge (2) to (4)), where the deep falling of the voltage is retarded for a while.

6.3.5 KiBaM battery model – simulations

The goal of this section is to analyse by simulations some aspects related with the KiBaM battery model, which was described in Section 4.2.2. These aspects are analysed having in mind the phenomena concerning battery behaviour, which have been observed in the measurements. It should be underlined that, for simplicity, the simulations here are done only on one single battery and not on an entire battery bank.

As no data are available for the installed battery, the 115Ah Dryfit A500 battery made by Sonnenschien was chosen for modelling and illustration purpose. For this battery, the data supplied by the manufacture are sufficiently comprehensive and can be directly used in the estimation of the parameters of the KiBaM model.

In Section 4.2.2, it was mentioned that the battery voltage is given by:

$$V_{bat} = E - I_{bat}\ R_0$$

where: E = internal battery voltage (open circuit voltage)
V_{bat} = battery voltage (alias terminal voltage of the battery)
I_{bat} = battery current
R_0 = battery internal resistance

KiBaM model contains two major parts (see Section 4.2.2): 1) capacity model 2) voltage model. The capacity model is characterised by three constants *k, c, q_{max}*. These parameters are estimated using the non-linear least square curve fitting method, based on test data from the manufacture. No other detailed tests on the battery are necessary. However, these manufactures' tests provide data over a wide range for the discharging currents, namely from a very little current of 5A to a very high current of 805A. Therefore, in order to make the estimation to be better conditioned (see Section 4.2.2), it is convenient to use the following normalised capacity:

$$F_{t_1,t_2} = \frac{q_{T=t_1}}{q_{T=t_2}} = \frac{t_1\, I_{T=t_1}}{t_2\, I_{T=t_2}}$$

where F_{t_1,t_2} represents the normalised capacity to that capacity which corresponds to the slowest discharge rate ($I_{T=t_2}$ smallest discharge current, t_2 biggest discharge time). $q_{T=t}$ denotes the discharge capacity at discharge time $T = t$ and discharge current $I_{T=t}$. t_1 corresponds to the actual discharge time, while t_2 corresponds to the biggest discharge time. $I_{T=t}$ denotes the discharge current to empty the battery in time *t:*

$$I_{T=t} = \frac{k\,c\,q_{\max}}{1 - e^{-k\,t} + c\,(k\,t - 1 + e^{-k\,t})}$$

The estimated parameters for the capacity model are:

$$\begin{aligned} k &= 2.2717\ [1/h] \\ c &= 0.3683 \\ q_{\max} &= 119.34\ [Ah] \end{aligned}$$

As it was mentioned, the value *c* reflects the fraction of the total charge in the battery that is readily available, while *k* indicates the rate at which the chemically bound charge becomes available. It is interesting to see that for a full new battery, only $36.83\,\%$ of the total charge represents the available charge. The predicted value $q_{\max}$ states the largest absolute value of the battery capacity at the limit of no discharge current. The 115Ah nominal capacity, which is indicated in the manufacture's data for the A500 battery, is the capacity corresponding to a 20h discharge current (5.75 A).

Figure 44 illustrates both the fitting of the current function to the Dryfit A500 battery data and the maximum permissible discharge current for the battery to prevent damage. It looks like that the fitting is quite good for currents under 120A. This fact fits in with the current range for a stand-alone PV system.

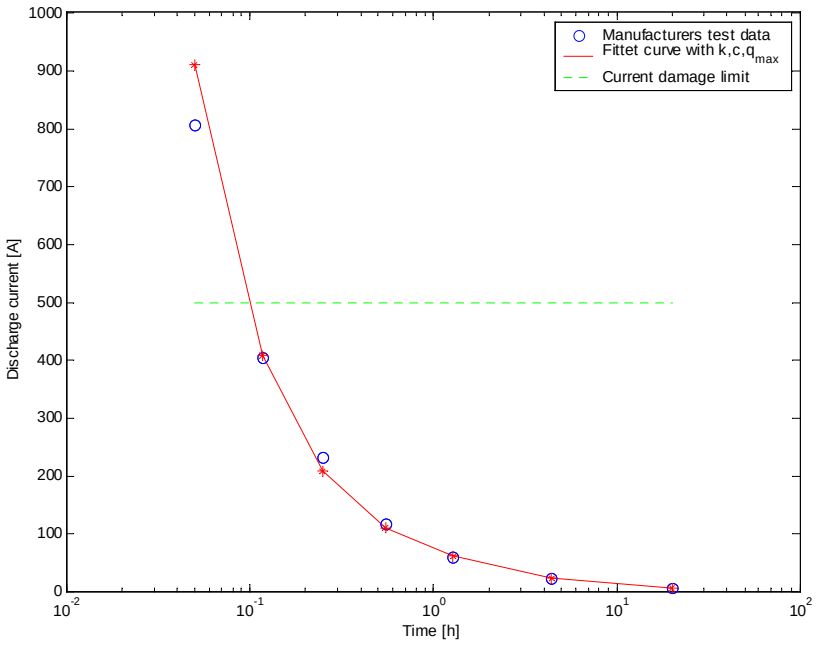

Figure 44: Discharge current as function of the discharge time.

As it was presented in Section 4.2.2, the KiBaM voltage model describes the voltage source E as function of the state of charge **SOC** and current:

$$E = E_0 + A\,X + C\,X\,/\,(D - X)$$

The terminal voltage E is function of the normalised capacity removed from the battery at a given discharge current. The normalised capacity X and the state of charge **SOC** are expressed by:

$$X = q_{out} \cdot \frac{q_{\max}}{q_{\max}(I)}$$

$$SOC = \frac{q_{\max} - q_{out}}{q_{\max}} = 1 - \frac{q_{out}}{q_{\max}}$$

where $q_{\max}$ is maximum possible capacity at $I = 0$ and $q_{\max}(I)$ is the maximum capacity at the present discharge current. The removed capacity is:

$$q_{out} = \int I_{bat}\, dt = q_{\max} - q$$

$$q = q_1 + q_2$$

where q_1 and q_2 denote the available and bounded capacity, respectively – see Figure 13. It is seen that the normalised capacity X is function of the removed capacity q_{out}, and thus function of the total capacity *q* of the battery.

Non-linear least square curve fitting is again used to find the voltage parameters E_0, A, C, D:

$$\begin{aligned} E_0 &= 12.5504 \text{ V} \\ A &= -0.0066 \text{ V/Ah} \\ C &= -0.3190 \text{ V} \\ D &= 134.1550 \text{ Ah} \end{aligned}$$

The voltage model also assumes that the internal resistance R_0 of the battery is constant. It is estimated to $R_0 = 0.0026\,\Omega$.

The open-circuit fully charged battery voltage E_0 indicates the maximum limiting voltage during discharge and the minimum limiting voltage during charge. Parameter A signifies the linear variation of the internal battery voltage *E* with the state of charge **SOC,** and as expected, it has a negative value in discharging. Parameter C indicates the decrease/increase of the battery voltage when the battery is progressively discharged/charged, and as expected it is negative in discharging. Parameter D reflects the sharp decrease in terminal voltage as the battery approaches the discharge limit. *D* is positive and approximately close to the maximum capacity $q_{\max}$.

Figure 45 shows the fitting of the terminal voltage E to the manufactures data. The fitting error appears insignificant in the co-linear range of the discharging curve. However, at the capacity limit $q_{\max} = 119.34$ Ah the error in the curve fit becomes more apparent. As the function $E = E_0 + A \cdot X + \frac{C \cdot X}{D - X}$ is injective, for $X = q_{\max}$ only one value is estimated for the terminal voltage E. It is

seen in Figure 45 that this value corresponds to the average of the data points located at $X = q_{\max}$.

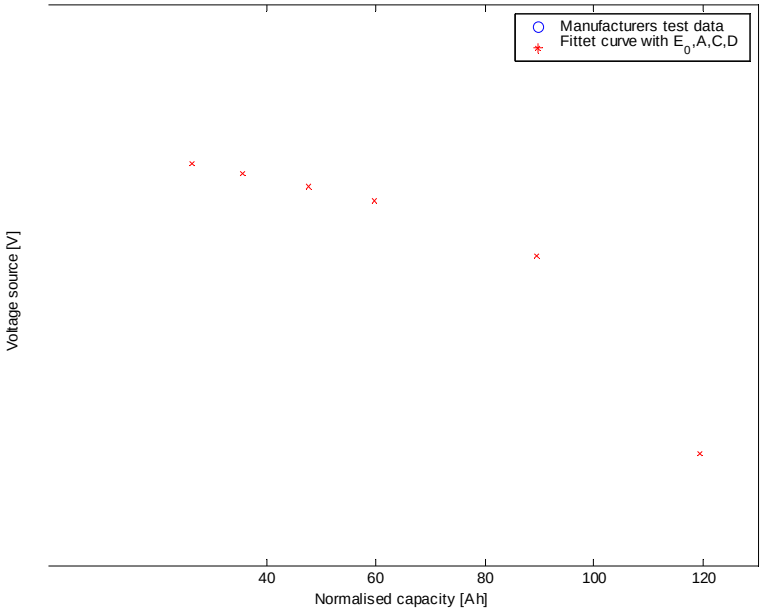

Figure 45: Battery voltage versus normalised capacity removed from the battery.

Once the KiBaM parameters ($k, c, q_{\max}$ for capacity model, E_0, A, C, D for voltage model and R_0) are thus estimated, the Simulink KiBaM battery model shown in Figure 22 can be applied.

First, a simple simulation of the KiBaM model is performed, in order to identify/illustrate the contribution of each component in the voltage model. For doing this, it is considered the case when the battery is discharged with constant current, i.e. $I_{bat}=30$ *A.* Figure 46 shows the influence on the battery voltage of each term in the expression for the battery voltage: E_0, A X and C $X / (D-X)$. As it was mentioned in Section 4.2.2, KiBaM battery model is able to predict the slowly decreasing of the battery voltage at the beginning of the discharge and the rapid falling of the battery voltage at the end of the discharge.

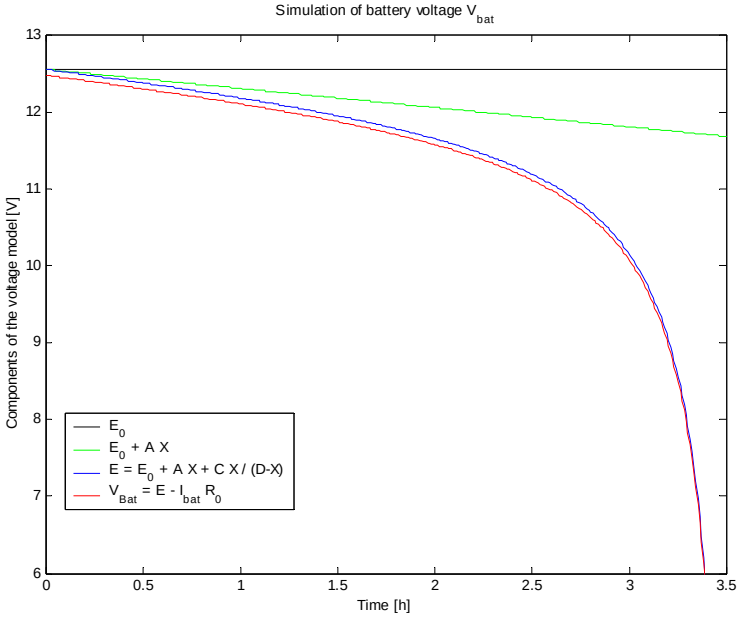

Figure 46: Contribution of the each component in the voltage model.

E_0 indicates the open-circuit fully charged voltage of the battery, while the term $A\ X$ reflects the linear variation of the internal battery voltage. It is seen that, when the discharge persists and thus when the normalised capacity removed from the battery increases close to $X \rightarrow D$, the term $C\ X\ /\ (D\text{-}X)$ generates the rapid drop in the internal battery voltage. The terminal voltage V_{bat} follows the variation of the internal voltage E, with the difference given by the constant term $I_{bat}\ R_0$.

The next step in the analysis is to illustrate, comparatively with the measurements, how the KiBaM model predicts the behaviour of the battery. A discharge strategy is thus simulated, under the following conditions:

- the battery is assumed to be full at the beginning of the discharging (**SOC**=1).
- the discharging alternates only with retrieving (i.e. no charging).
- the discharge current sequence is similar to that accounted in the measurements, namely it is constant at 0A during 1.5 hours retrieving and constant at 30A during 15 minutes discharging.

Note that the simulation data corresponds to that of a single battery and not to the entire battery bank.

Figure 47 illustrates the simulated discharging current and the corresponding battery voltage, while Figure 48 presents the state of charge **SOC**, the removed capacity $q_{out} = \int I_{bat}\ dt$ and the normalised capacity $X = q_{out} \cdot \frac{q_{\max}}{q_{\max}(I)}$.

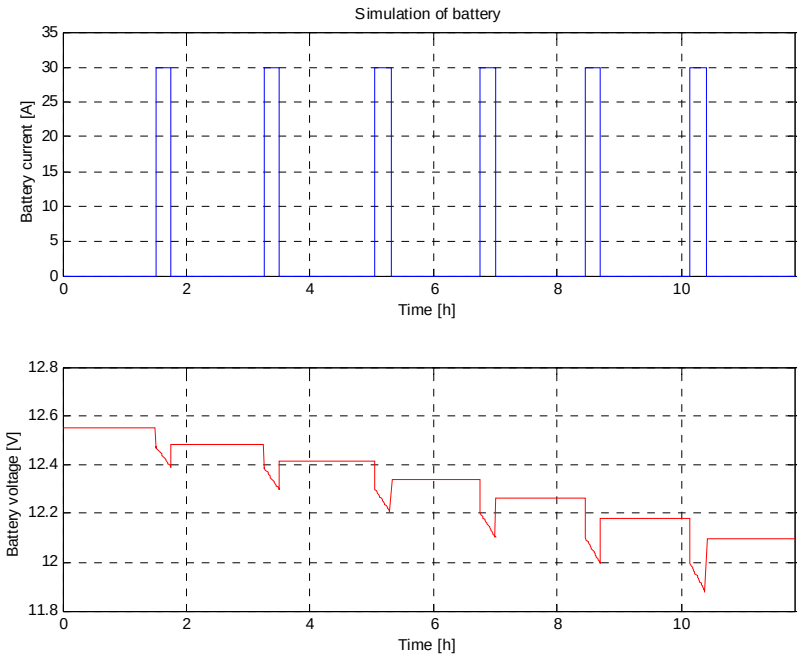

Figure 47: Battery current and simulated battery voltage using the KiBaM model.

The following summarises a number of observations on the KiBaM model:

1) First, it is noticed that the KiBaM model does not reflect the retrieving process, existing in the battery voltage, when the current becomes zeros after a discharge – see Figure 47. After discharging, the step in current to zero results in a step in the battery voltage and not to a slow increasing - as it was seen, for example, in Figure 34.

2) It is observed that the model does not reflect the internal dynamic behaviour of the battery, during a progressive discharging. In Section 6.3.4, it was illustrated by measurements that the battery has a non-linear dynamic behaviour, visible especially during progressive discharging. This behaviour is not observed likewise in the KiBaM simulation.

3) It can be seen that the KiBaM model predicts the ”voltage level stairs” corresponding to different retrieving levels. This is a sign that the state of charge **SOC** becomes lower with each discharging. Figure 48 illustrates how the state of charge **SOC** is decreasing during discharge, and it is remaining constant during retrieving.

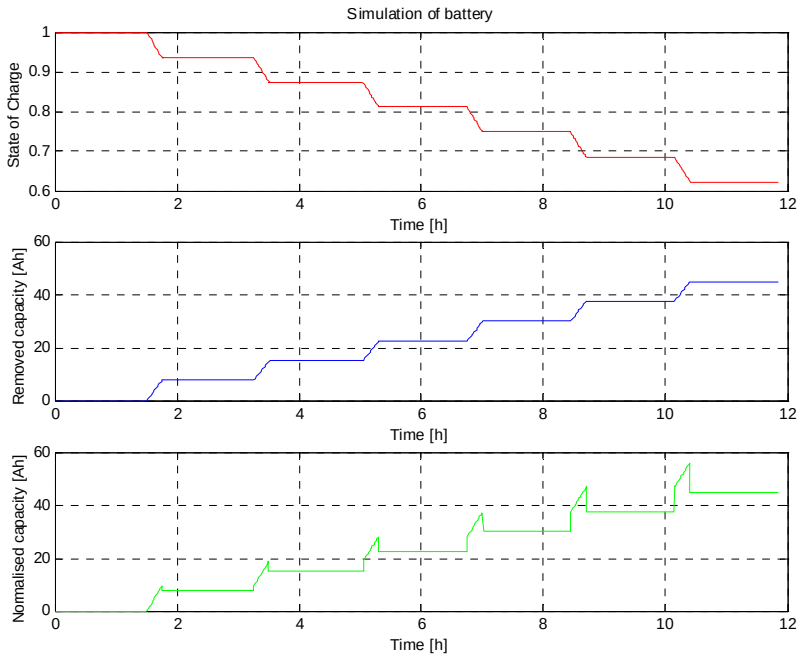

*Figure 48: Simulated state of charge **SOC**, removed capacity q_{out} and normalised capacity X .*

It is also seen that during discharge, the removed capacity q_{out} is increasing, as being an integration of the discharging current $I_{bat} > 0$. As expected, the normalised capacity $X = q_{out} \cdot \frac{q_{\max}}{q_{\max}(I)}$ "follows" the removed capacity q_{out} :

- during retrieving $I_{bat} = 0$, then $q_{\max}(I) = q_{\max}$ and thus $X = q_{out}$ (during retrieving X and q_{out} have the same level in Figure 48).
- during discharge $I_{bat} > 0$, then $q_{\max}(I) < q_{\max}$ and thus $q_{out} < X < q_{\max}$. During discharge, the normalised capacity X takes the form of a "shark fin" – see Figure 48.

4) It is observed that even though the value of the simulated discharge current I_{bat} is the same over the whole discharging sequence, the "shark fin" becomes bigger and bigger, as the number of the discharge regimes is increased –see Figure 48. This aspect is illustrated in the battery voltage by the deeper and deeper "upside down shark fin" – see Figure 47. This phenomena, seen both in KiBaM simulations and in measurements – see Figure 34, underlines that the deeper instantaneous jumps in the battery voltage $V_{bat} = E - I_{bat} \cdot R_0$ due to the steps in the battery current, are not the result of a variable internal resistance R_0, as it was assumed in Section 6.3.2, but more likely of the normalised capacity *X* of the battery.

5) The state of charge **SOC** is reflected by the step level in the battery voltage, while the normalised capacity *X* is related with the step response, due to the term $q_{max}(I)$.

6) In KiBaM model, only the external dynamic behaviour of the battery is visible. The internal dynamic behaviour of the battery, reflected for example in the available q_1 or the bounded capacity q_2, is hidden. The reason for this is that the

internal voltage E is function of the normalised capacity X, and thus function of the total capacity q of the battery, and not function of q_1 or q_2.

Figure 49 illustrates the variation of the available q_1, bounded q_2 and total capacity q, used in KiBaM model. It is observed that while both q_1 and q_2 has a dynamic behaviour, the total capacity q (sum of the available and bounded capacities) does not contain any dynamics at all. It is seen how the available capacity q_1 decreases during discharging and slowly increases when retrieving. This dynamic behaviour of q_1 is similar to the behaviour of the battery voltage in the measurements, being not present in the simulated battery voltage – see Figure 47. It is also seen that the bounded capacity q_2 behaves as an integrator state without any information control from outside.

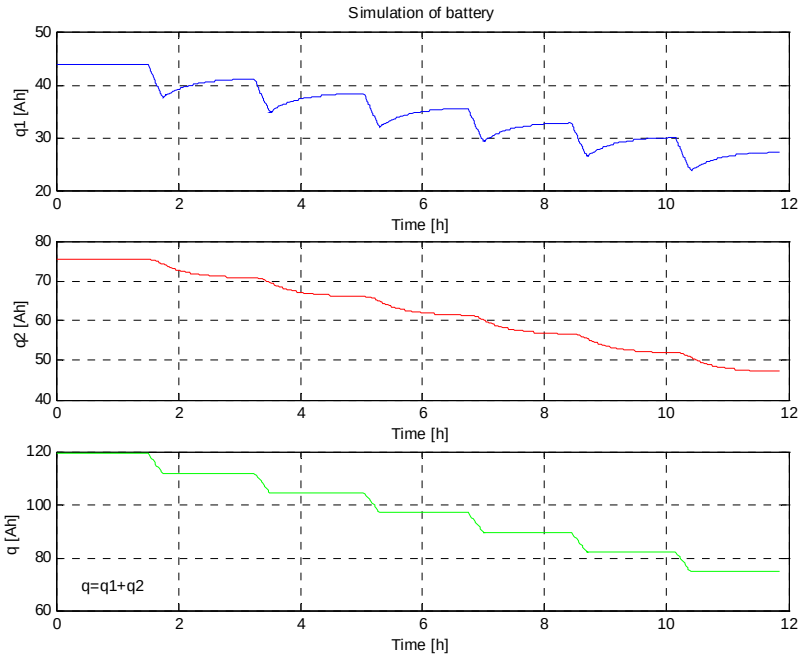

Figure 49: Available q_1, bounded q_2 and total capacity $q = q_1 + q_2$ of the battery – simulation.

It seems that q_1 and q_2 supplement each other, as their sum q does not contain any internal dynamic.

Thus, the internal dynamic of the battery is hidden and only the external dynamic of the battery is visible in KiBaM model. The voltage of the battery should not be described only based on the current flow through the battery, but also by the internal dynamic/structure. The present model formulation of the KiBaM model is only adequate for long term simulations. For short-term simulations where the dynamic behaviour of the battery voltage is of higher importance, it can be concluded that the KiBaM model is not good enough.

It is thus expected that the battery model can be improved by describing the internal voltage E as function of the internal dynamic. This means that it should be expressed as function of the bounded capacity q_2 or of the available capacity q_1, and not as function of the total capacity q, as it is done in KiBaM model.

6.4 Controller model validation

It should be mentioned that, before the acquirement of the measurement data on the stand-alone PV system at Risø, there was no prior available knowledge about the dispatch strategy of the controller in the whole PV system. Thus, information about the controller system has been achieved based only on the analysis of the measurements. It is concluded that there are indirectly two independent controllers:

- PV controller
- Inverter controller

It seems that, in the PV system at Risø, there does not exist a load controller (discharge controller) to protect the battery against excessive discharge.

The PV controller acts only on PV arrays, connecting or disconnecting them gradually –see scheme in Appendix C. A disconnection of the PV arrays, due to the high irradiation and to the overcharged battery, was illustrated for example in Figure 25. A zoom on this disconnection is done and presented in Figure 50. It is seen that, in order to avoid overcharging, the PV controller disconnects the PV arrays, when the battery voltage reaches the limit of the charging voltage V_{max_off} = 27V. The PV controller reconnects the first array later, when the battery voltage decreases toV_{max_on} = 24.7V.

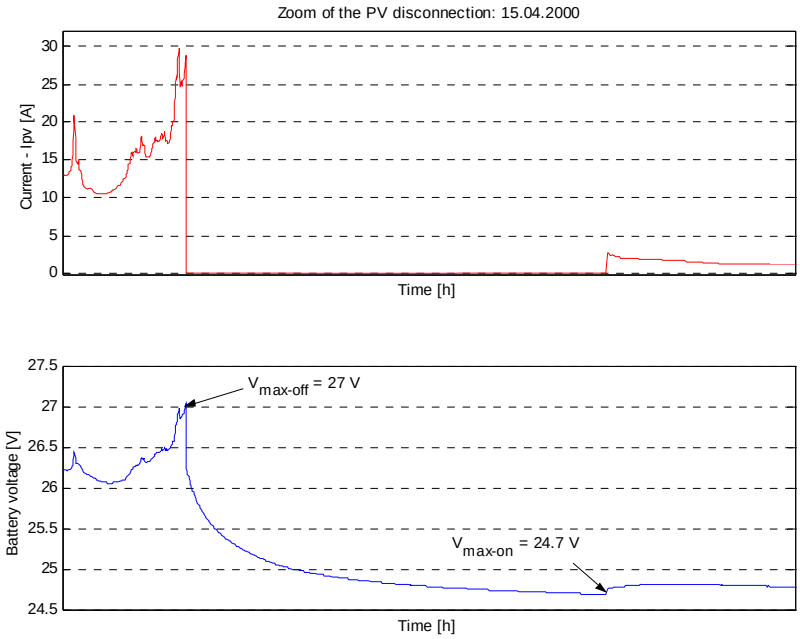

Figure 50: Focus on the voltage limits of the PV controller in connection/ disconnection of the PV arrays.

These values V_{max_off} and V_{max_on} are used in the Simulink implementation of the dispatch for the overcharge protector, which is based on a hysteresis, as presented in Figure 14. Based only on the measurements, it is difficult to determine the moments when the other three PV arrays are connected/disconnected gradually to/from the system.

It is also found out that the inverter in the stand-alone PV system at Risø is supervised by its own controller, which connects/disconnects the load, when the

voltage on the DC-side of the inverter is above or below a critical value. Figure 51 illustrates a zoom on the load connection/disconnection done by the inverter controller.

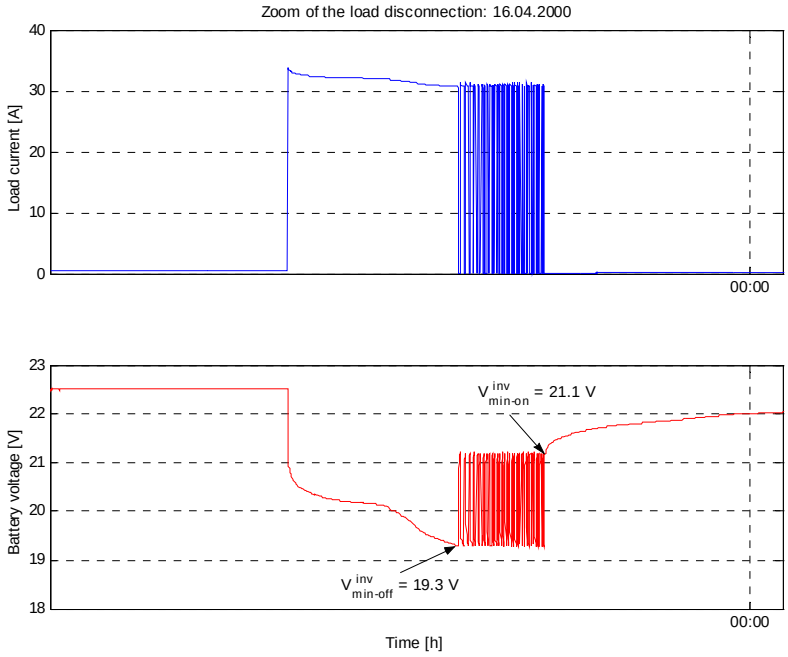

Figure 51: Focus on the voltage limits of the inverter controller in connection/disconnection of the load.

There are indicated the critical values when the inverter controller disconnects/connects the load to the stand-alone system. Thus, the load is disconnected when the DC voltage reaches the critical low value $V_{\min\_off}^{inv} = 19.3\,\mathrm{V}$. This estimated value $V_{\min\_off}^{inv}$ is in concordance with the value of 19V, presented in the manufacture data sheets, available on the inverter. The load is reconnected by the inverter controller when the DC voltage comes up to $V_{\min\_on}^{inv} = 21.1\,\mathrm{V}$. The implementation of the inverter controller is based on a hysteresis, similar to that presented in Figure 18.

6.5 Inverter model validation

In Section 4.5, the efficiency of the inverter is defined as:

$$\eta = \frac{P_{out}}{P_{in}} = \frac{P_{ac}}{P_{dc}} = \frac{P_{ac}}{V_{dc} \cdot I_{dc}}$$

where P_{ac} is the measured power on the AC-side of the inverter, while P_{dc} is the power on the DC-side of the inverter. The DC-voltage is $V_{dc} = V_{bat}$, while the DC-current is $I_{dc} = I_{load}$ (see Table 4).

The inverter has only two operating modes (load or not), which can be switched by an ”on-off” button. In order to estimate the efficiency of the inverter, it is necessary to expose the system to different loads and therefore to perform the measurements on the inverter using a variable load. It should be mentioned that

in the determination of the inverter efficiency, the constant load (the electrical heater) is completely disconnected. Instead, the variable load consisting of seven identical bulbs of 60W is applied by gradually increasing the number of bulbs. In each step P_{ac}, V_{bat} and I_{load} are measured.

A linear regression is performed on the measured signals, using the expression:

$$P_{ac} = \alpha \cdot P_{dc} + \beta$$

where α accounts for the load dependent losses and β indicates the no-load losses. These parameters have been estimated to $\alpha = 0.905$ and $\beta = -2.33\,\mathrm{W}$. As $\eta = \alpha + \beta / P_{dc}$ and $\beta << P_{dc}$, it can be approximated that the rated efficiency is $\eta \cong \alpha = 0.91$. Figure 52 illustrates both the measurements and the estimated linear regression.

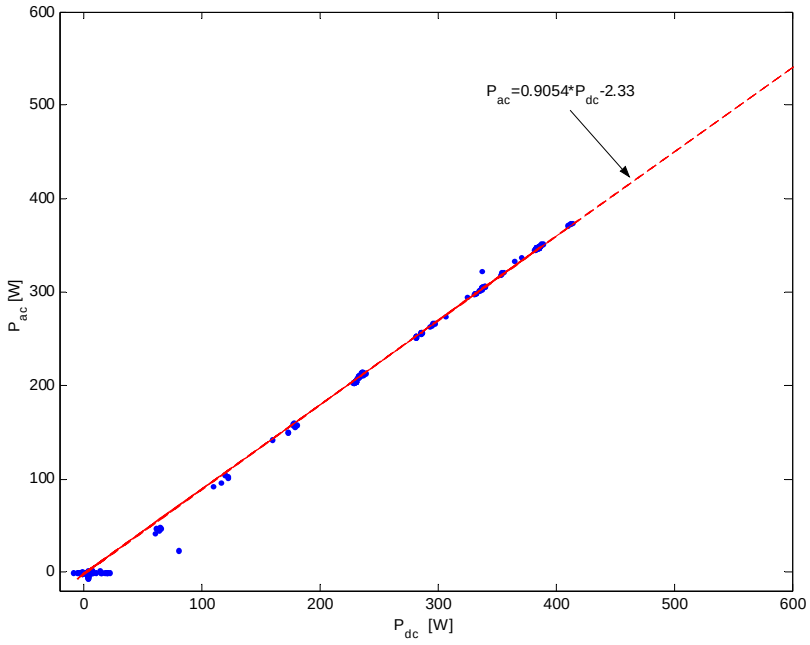

Figure 52: Measurements and the estimated efficiency of the inverter.

It is noticed that the measurements, presented in Figure 52, are gathered in seven groups of 4-5 measurements per group. This corresponds to the gradually increasing number of connected bulbs, having 4-5 samples connected bulb per group. The estimated efficiency $\eta = 0.91$ is in agreement with the value of the efficiency indicated in the manufacture data sheets, namely of 92%.

Once the efficiency η is estimated, it can be used directly in the model of the inverter, presented in Section 4.5. Thus, knowing the current I_{ac} and the voltage V_{ac} on the AC-side of the inverter, the voltage on DC-side V_{bat} and the efficiency η, the current I_{load} can be simulated with the Simulink model – see Section 5.2.

7 Dynamic modelling of the battery

In Section 4.2, an approach of modelling the battery was described. The applied model was derived from an equivalent water storage system with two compartments. This model was found to have an insufficient modelling of the faster dynamics, Section 6.3. In this section, the modelling will be based on Black box models, i.e. linear time discrete linear models – although the battery behaviour is quite non-linear. This modelling approach is used to analyse measurement data from the battery in order to achieve a better understanding of the battery dynamics.

7.1 Black box approach

Modelling of dynamic systems is also referred to as System Identification. The Black box modelling approach is a well-established technique in modelling dynamic systems. Quite a number of books have been written on this subject, e.g. (Box & Jenkins, 1976), (Soderstrom & Stoica, 1989), (Ljung.L, 1999), (Madsen, 1995). Therefore, only a short introduction to this time discrete approach is presented below, where essential keywords are introduced.

A first step in the modelling of a dynamic system is to select a proper model description for the system to be modelled. Different model structures exist with respect to parametric, spectral and correlation model descriptions. Next step is to select an appropriate estimation method – depending on the selected model type – and to estimate the parameters. Finally, the model performance must be validated in order to decide whether the model can model the system.

In this modelling approach a linear state space structure (parametric model) is applied for the following reasons:

1) it is assumed that given knowledge on the present state of the battery at time t_0 is available. This knowledge combined with knowledge on future input signals and disturbances will unambiguous determine the state of the battery at $t \geq t_0$. This property is related to a Markov process property, which justifies the use of a state space structure. Moreover, the state space structure will reveal knowledge about the underlying dynamics, if the states can be interpreted.
2) the model structure is assumed to be linear – despite the facts reported in Section 6.3 – as it makes the estimation method less complex compared to non-linear estimation methods.
3) the description is chosen parametric as it makes comparisons to the KiBaM model more feasible, see Section 4.2 and Section 6.3.

An advantage of using a Black box modelling approach compared to e.g. a Grey box modelling approach is that no prior system knowledge is necessary. However, it is usually difficult to interpret the estimated parameters (at model orders higher than 3) by equivalent physical parameters. On the other hand, if the system is fairly well known, it would be more advantageous to apply a Grey box modelling approach, see e.g. (Hansen, 1997), where estimation of continuous time parameters in non-linear models is performed.

7.1.1 Parametric models using linear state space structures

The Identification Toolbox in Matlab offers a handful of model structures for parameter estimation, e.g. ARX models, ARMAX models, FIR models, Box-Jenkins models (which all are output-error models) and state space models (prediction error model), refer to (Ljung, 2000). The state space structure is selected due to the related estimation method, i.e. the prediction error method. The prediction property imposes quite high demands to the model and to its performance – compared to an output-error model. If the modelling succeeds, the resulting model supports physical understanding of the dynamics of the modelled system. Furthermore, in some cases it is even possible to find physical interpretation of the time discrete parameters.

The basic state space model in innovations form – implemented in Matlab – can be written as:

$$x_{k+1} = A\,x_k + B\,u_k + K\,e_k$$
$$y_k = C\,x_k + D\,u_k + e_k$$

where x_k denotes a vector with the states of the system, u_k is a vector of system inputs, y_k is a vector of the measured system outputs and e_k denotes a noise source – all at time k. The order of the system is equivalent to the number of state, i.e. the length of x_k. The matrices A, B, C, D and K contain all the parameters of the system. E.g. element $a_{i,j}$ of matrix A is a parameter, which defines the relation between state x_i at time k and state x_j at time k+1. Matrix K determines the disturbance properties of the system. If K is zero, the noise source e only effects the output y. Thus the model is reduced to an output error model.

In this context, u_k is a scalar, which represents the battery current. y_k is also a scalar, which represents the battery voltage. The state vector x_k contains internal battery states. At model order 2, this model is almost similar to the KiBaM model.

7.1.2 Estimation method

A standard prediction error/maximum likelihood method, based on iterative minimisation of a criterion is used, (Ljung.L, 1999). The iterations are started from parameter values that are computed from N4SID, (Ljung, 2000). The parameterisation of the matrices A, B, C, D, and K is free and adjusted to be numerically well conditioned.

7.1.3 Validation methods

Model validation is an import part of the modelling process. The purpose of the validation is to assess: 1) the performance of a suggested model and 2) the parameter estimates, i.e. whether or not an estimated model satisfies a number of posed criteria.

The model performance will in this context be validated by two methods:

1) residual analysis.
2) cross validation.

refer to (Madsen, 1995) or (Hansen, 1997) for further information.

Residual analysis is in this context a visual inspection of the residuals – looking for zero mean and constant variance (Holst et al., 1992) – and verification of the

autocorrelation and crosscorrelation functions. The cross validation procedure is a method to investigate/test the generalisation properties of a parameter estimate given a model structure. The method is based on two data sets – one is used for estimation of the parameters while the other is used in a simulation applying the estimated parameters. Next step is to compare the variance of the prediction errors. If these variances are of equal size, the estimated parameters are presumably equal to the optimal parameters. If not equal, the parameters are either related to a local optimum or the model is not adequate.

7.1.4 Estimation results and validation

Sequences of the two data sets, *set2data* and *set3data*, presented in Section 6.3 are used below. The applied sequences are the data, which were presented in Figure 34 and Figure 42, respectively. From these two figures it can be observed that the voltage variation in *set3data*, see Figure 42, covers a bigger range than that of *set2data*, see Figure 34. Thus, the selected sequence of *set3data* contains more information on the non-linear behaviour of the battery. Therefore, the selected sequence of *set3data* is used for estimation, while the selected sequence of *set2data* is applied for the cross validation. It should be noticed that since the applied model structures are linear, the mean value of the input (the battery current) and the output (the battery voltage)

The Identification Toolbox operates with an internal measure, which is the percentage of the output variations that is reproduced by the model. It is calculated as:

$$\mathrm{Pss} = \left(1 - \frac{|\,y - \hat{y}\,|}{|\,y - \bar{y}\,|}\right) \cdot 100$$

where y is the measured output, $\hat{y}$ is the simulated/predicted model output and $\bar{y}$ is the mean value of y. If y and $\hat{y}$ are approximately similar the norm |x| will be small. Thus, a higher number of Pss indicates a better model.

In order to be able to evaluate the influence of the sample frequency, a number of estimations have be performed at different sample frequencies, i.e. the original measurement data (at one second) have been sub-sampled by a factor as shown in Table 6.

Table 6. Model performances from estimation with the selected sequence of set3data *using the Pss-measure. The number in brackets is used to rank the estimated models.*

Pss	**Sub-sampling factor**					
order	None	10	30	60	90	120
1	30.4829 (5)	38.1448 (5)	38.1069 (6)	37.9853 (6)	37.8821 (6)	-138.2626 (5)
2	41.1844 (3)	62.0720 (1)	62.3255 (2)	60.7612 (4)	59.0776 (5)	-39.7911 (4)
3	61.2897 (2)	58.8990 (3)	62.7137 (1)	59.4817 (5)	61.3560 (2)	47.9617 (1)
4	61.7136 (1)	58.1895 (4)	58.5020 (4)	60.9407 (3)	61.1219 (3)	-24.9995 (3)
5	30.4829 (4)	61.7923 (2)	60.6934 (5)	64.5526 (2)	67.3602 (1)	-12.6795 (2)
6	–	–	61.9282 (2)	66.9837 (1)	59.0819 (4)	–

In optimisation, there is always a risk of entering in a local optimum. Hence, interpretation on the numbers in Table 6 must be made with caution, as the estimation results are the outcome of optimisations. Expectation is that a higher model order will perform a better fit due to the higher degree of freedom. On

the other hand, the number of parameters to be estimated increases with model order. Thus, the risk of hitting a local optimum is increased.

In Table 7, a crosschecking of performance using the Pss-measure is shown – again performed at different sample frequencies.

Table 7. Cross-checking model performances from simulation with the selected sequence of set2data using the Pss-measure. The number in brackets is used to rank the estimated models.

Pss	**Sub-sampling factor**					
order	None	10	30	60	90	120
1	28.1019 (5)	10.6050 (5)	10.2910 (6)	9.8404 (6)	9.4259 (6)	-102.9425 (5)
2	51.1702 (4)	57.3782 (3)	56.6424 (3)	54.3497 (3)	52.6170 (4)	-22.3827 (4)
3	58.5201 (1)	67.6326 (1)	53.9621 (4)	55.8485 (2)	49.2055 (5)	37.3132 (1)
4	58.0958 (2)	65.9301 (2)	53.9511 (5)	58.9433 (1)	53.5026 (2)	4.0957 (2)
5	54.7453 (3)	57.3782 (4)	60.4204 (1)	46.5667 (5)	53.2768 (3)	-6.7570 (3)
6	–	–	56.9485 (2)	50.1825 (4)	57.3413 (1)	–

From Table 6 it can be observed that sub-sampling the data with a factor 120 – i.e. from 1 second to 2 minutes – significantly reduce model performance. The same conclusion goes for Table 7. Moreover, a significant improvement in model performance is achieved by increasing the model order from one to two. A visual inspection of the numbers in Table 6 and Table 7 combined with comparison of the two sets of numbers leads to the conclusion that a sub-sampling factor of 10, 30 or 60 – alias sampling times of 10 seconds, half a minute or one minute – is a fair choice.

The best simulation performance with the selected sequence of *set2data* happens to be the model at a sub-sampling factor of 10 (i.e. 10 seconds sampling time) of order 3, see Table 7. Therefore, this model has been chosen for further analysis with respect to the methods presented in Section 7.1.3. The estimated parameters of the 3rd order linear model are as follows:

$$x_{k+1} = \begin{bmatrix} 0.99756 & -0.01477 & 0.02873 \\ -0.01879 & 0.85304 & 0.44 \\ 0.00373 & 0.02764 & -0.62148 \end{bmatrix} x_k + \begin{bmatrix} -0.00111 \\ -0.01584 \\ 0.05103 \end{bmatrix} u_k + \begin{bmatrix} 0.00826 \\ 0.13266 \\ -0.05835 \end{bmatrix} e_k$$

$$y_k = \begin{bmatrix} 65.569, & -0.41333, & 0.31428 \end{bmatrix} x_k + e_k$$

with $x_0=[0.00018428, 0.062485, 0.043433]^T$. It is noted that the D matrix is to zero. The eigenvalues of the matrix A (alias the poles of the equivalent transfer function) are: 0.9995, 0.8594 and -0.6298.

The model performance with the selected sequence of *set3data* at a sub-sampling factor of 10 is shown in Figure 53. The black line is the measurement of the battery voltage, while the coloured lines illustrate model output at different model orders. A visual inspection reveals that a significant improvement in model performance is achieved by increasing the model order from one to two. It can be observed in the last half of the figure that the lower and lower battery voltage implies a bigger and bigger deviation between measurements and all model outputs. This implies that the dynamics of the battery is more non-linear at the low battery voltages.

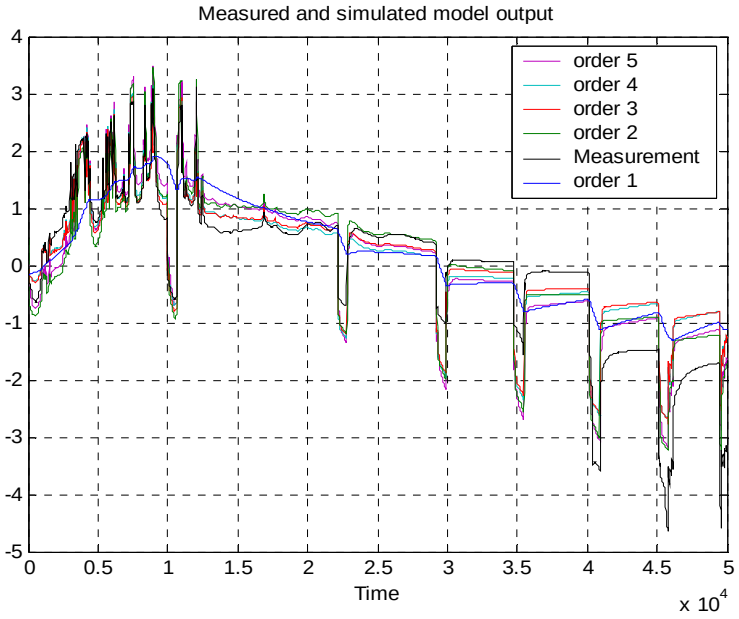

Figure 53. Model performances with the selected sequence of set3data *at a sub-sampling factor of 10. Best fits: model of order 2.*

The residuals (difference between measurement and model) of order 3 is plotted in Figure 54. If the model was capable of modelling the measurement, the residuals would have zero mean, constant variance (i.e. be white noise) and be uncorrelated. This is not the case. The remark on Figure 53 with respect to the non-linear behaviour becomes even more evident in Figure 54.

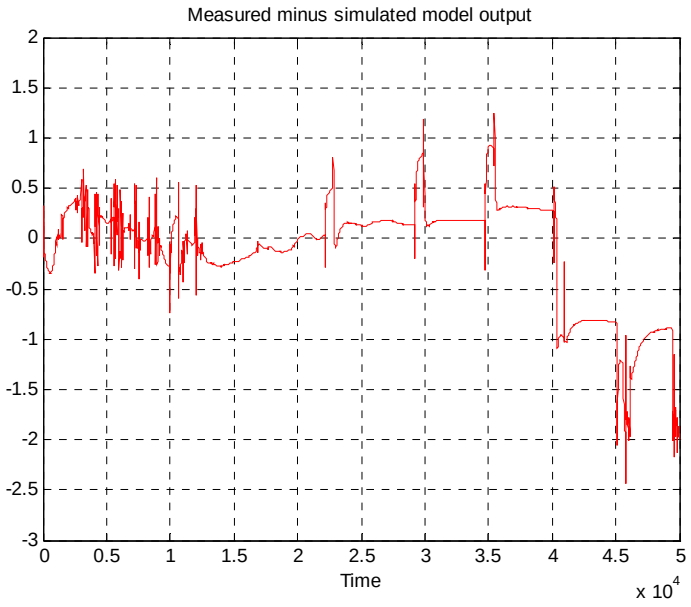

Figure 54. Residuals of model order 3 at a sub-sampling factor of 10.

As stated above the residuals are not white noise. If the model performance had been much better, it could have been difficult to see whether or not the nature of the residual was white noise. In this case, an inspection of the autocorrelation of the residuals and the crosscorrelation between the input (the battery current) and the residuals could be used to analyse the actual situation. The autocorrelation and the crosscorrelation related to Figure 54 are shown in Figure 55. The red

dashed lines indicate the 99% confidence intervals. The autocorrelation and the crosscorrelation may not cross these lines. If the do the residuals are not white noise. The crosscorrelation indicates that the input part of the model can be improved.

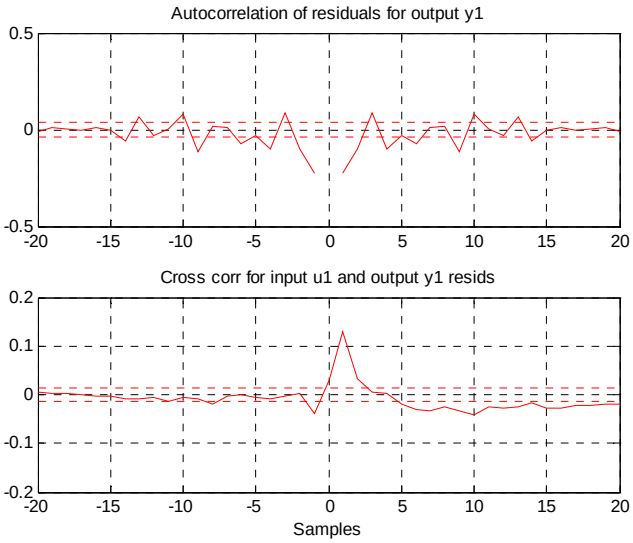

Figure 55. Auto- and crosscorrelation functions with respect to the prediction error with respect to Figure 54.

The eigenvalues of matrix A in the state space structure can of course be calculated based on the estimated parameters. This idea is the essential contents of Figure 56, where the location of the zeros and poles of a transfer function description equivalent to state space description are plotted. In this particular case, one pole is placed in $z \approx 1$, which is equivalent to an integration. Inspection of all the estimated models have shown that they all have this property. This is actually similar to the KiBaM model, which also contains an integration.

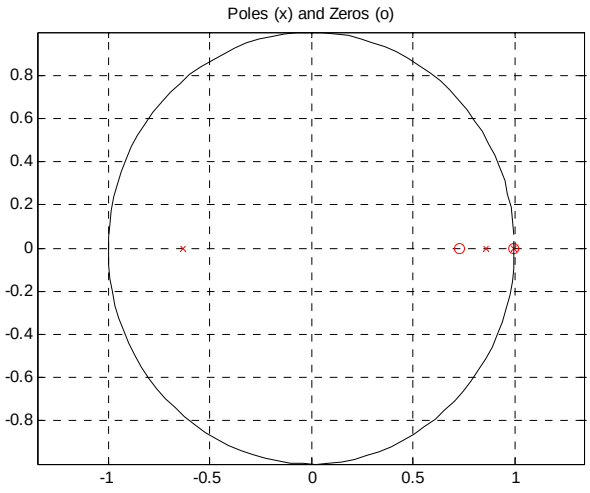

Figure 56. Location of poles and zeros.

As described in Section 7.1.3, the model performance can also be validated by a cross validation. The results are presented in Table 8. It can be observed that no

set of variances is of equal size – which without too much surprise indicates that the models are inadequate. As seen before a significant improvement is achieved going from model order 1 to order 2. It should be noticed that no significant improvements are achieved going from model order 2 to order 3, etc.

Table 8. Cross validation performances using the variances of the prediction errors from estimation with the selected sequence of set3data *and simulation with the selected sequence of* set2data.

order	sub-sampling factor: 10		sub-sampling factor: 30		sub-sampling factor: 60	
	estimation	simulation	Estimation	Simulation	estimation	simulation
1	0.5906	0.3631	0.5905	0.3651	0.5895	0.3669
2	0.1975	0.0880	0.2082	0.1034	0.2270	0.1156
3	0.2596	0.0516	0.2266	0.1027	0.2682	0.1134
4	0.2936	0.0591	0.2838	0.1044	0.2753	0.0993
5	0.2525	0.1016	0.2512	0.0791	0.2112	0.1435
6	–	–	0.2373	0.0903	0.2257	0.1440

Finally, the model performance from simulations with the selected sequence of *set2data* is plotted in Figure 57. Again, the black line is the measurement of the battery voltage, while the coloured lines illustrate model output at different model orders. The remarks made on Figure 53 can also be made on Figure 57.

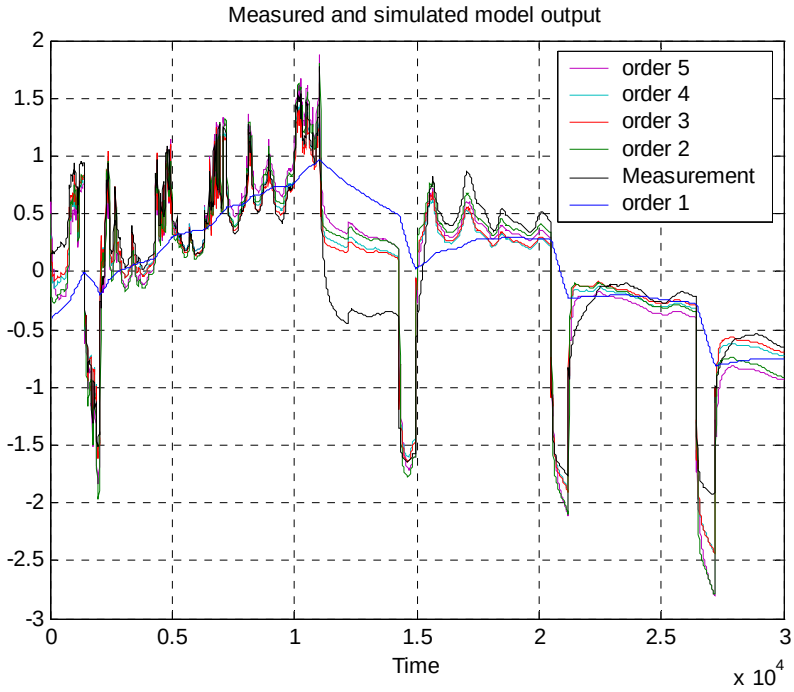

Figure 57. Model performance from simulations with the selected sequence of set2data. *Best fit: model of order 3.*

7.2 Modelling results

The modelling approach based on linear state space structures did not result in a sufficient modelling of the battery – i.e. the dynamic relation between battery current and battery voltage – the battery dynamic is simply too non-linear. Nevertheless, the performed modelling has added/confirmed a number of valuable informations on the battery dynamic:

- A proper sample time approximately is in the range of 10 to 60 seconds.
- At least a second order model should be applied.
- The model should contain one integrating state.
- The non-linear behaviour seems to be stronger at lower battery voltages compared to higher battery voltages.

The KiBaM model covers more or less these properties. It is a second order model with one integrating state. It has a non-linear description of the internal battery voltage with the most non-linear parts at very high and very low voltages.

In Section 6.3 the KiBaM model was tested by a simple discharge pattern. The estimated linear state space model using the selected sequence of *set3data* of model order 3 and 10 as sub-sampling factor has been exposed to the same current signal. The resulting simulation is shown in Figure 58 together with the simulation of the KiBaM model. As it can be observed in the figure, the voltage discharge depth is much bigger in case of the linear model. Moreover, the linear model has a dynamic response during zero current – a property, which is not reflected by the KiBaM model. Thus, the model description of KiBaM model should be slightly modified as mentioned in Section 6.3.

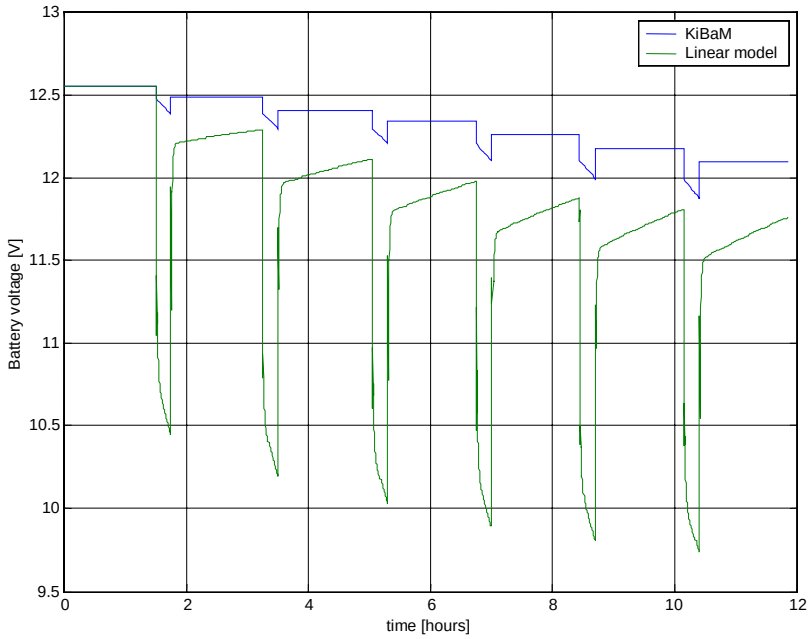

Figure 58. Comparison between simulation performance of the KiBaM model and the linear 3rd order state space model estimated at a sub-sampling factor of 10.

In future experiments it could be of interest also to measure the battery temperature in order to learn more about the dynamics.

8 Results and conclusion

The aim of this report was to provide insight into the modelling and simulation of a stand-alone PV system. A library of modular mathematical models was developed for each individual element of a stand-alone PV system, namely solar cells, battery, controller, inverter and load. Such a collection of simulation models (created in Simulink – Version 5) is a suitable tool for a further development and investigation of the dynamic behaviour of the PV system.

The validation of these mathematical models was performed through the comparison between the simulation results and the measurements, acquired from the stand-alone PV system at Risø. The validation of each individual component model has concluded the following remarks:

- PV module model: It reflects properly the influence of the irradiation and of the cell temperature on the I-V characteristic of the PV module. For the particular simulation, based on the rated data of the PV module, (supplied by the manufacture) and not on the specific measured data for the module, it was observed that the simulated efficiency was higher than the measured efficiency with almost 15%. The most likely explanation is that the efficiency of the panels is actually less than the rated values, e.g. measurements are acquired in realistic weather conditions, i.e. with panels subjected to dust etc. It seems that the model should be cautiously used for the case of extremely high irradiation (above 1000 W/m^2), high ambient temperature and high operating voltage. The simulation of the PV model could be perhaps also improved by using a direct measurement of the cell temperature and not an approximated value of it.
- Battery KiBaM model: It is adequate for long term simulations, but not for short-term simulations, where focus is on the dynamic behaviour of the battery voltage. The model is able to predict both the "voltage level stairs", corresponding to different state of charges **SOC**, and the sharp drop in voltage when the battery is nearly empty**.** However, it does not provide a sufficient description of the fast non-linear dynamic behaviour, observed in the measurements. Results from the Black box modelling indicate a model order of 2 and one integrating state. These features are present in the KiBaM model. However, contrary to the Black box model, the KiBaM model does not reflect the retrieving process. This indicates that, the KiBaM model could be improved by using in the voltage equation another variable than the total capacity. This new variable should reflect the internal dynamic behaviour of the battery.
- Controller model: No prior available knowledge about the dispatch strategy of the controller for the whole PV system, at Risø, was available. However, it was found out that there is no a protection of the battery against excessive discharge. The PV system has two controllers, one acting on the PV arrays to avoid the overcharging of the battery, and one acting on the inverter when the voltage on the DC side of the inverter becomes too low. The critical voltage values for the implementation of the controller dispatch have been identified based on measurements.
- Inverter model: The efficiency of the inverter, estimated based on the measurements, was in agreement with the value of the efficiency indicated in the manufacture data sheets.

Concerning the future work in the field of stand-alone system, this study revealed that there is a need for:

1. a better understanding and modelling of the highly non-linear dynamics of the battery. Systematic battery tests are necessary to get more information on how to improve the model of the state of charge **SOC** and of the dynamic in the battery voltage. The influence of the temperature on the battery is also an interesting issue to be studied.
2. a further analysis of the PV model concerning the simulated efficiency of the modules, the approximated cell temperature and the sensitivity of the PV modules performances as e.g. real life conditions and ageing of the cells.
3. over/under charging/discharging strategy protection in the control system.
4. tests for complete PV system viewed as a whole and not as individuals components.

Appendix A: Measurements

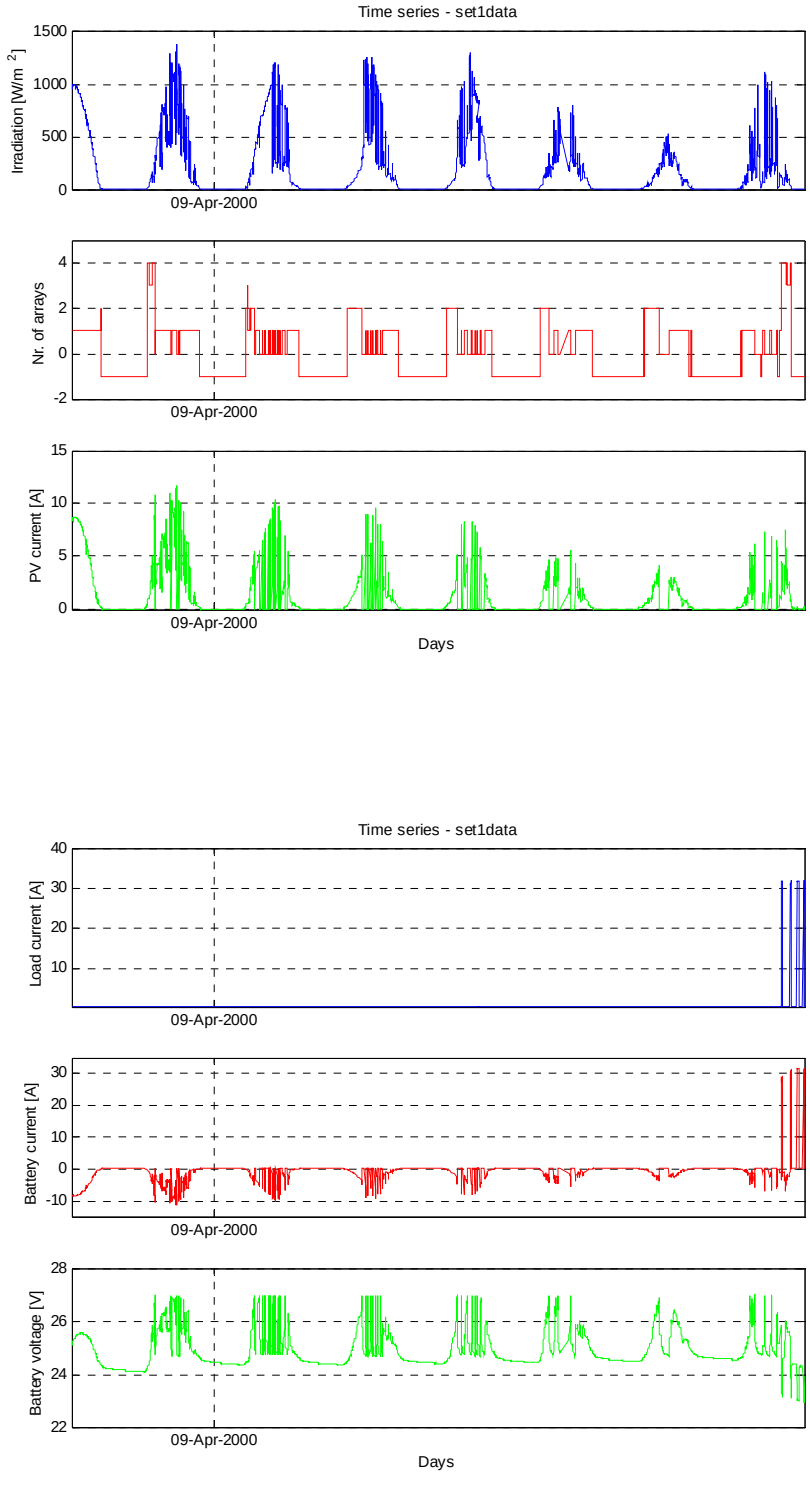

Figure 59: Set1data

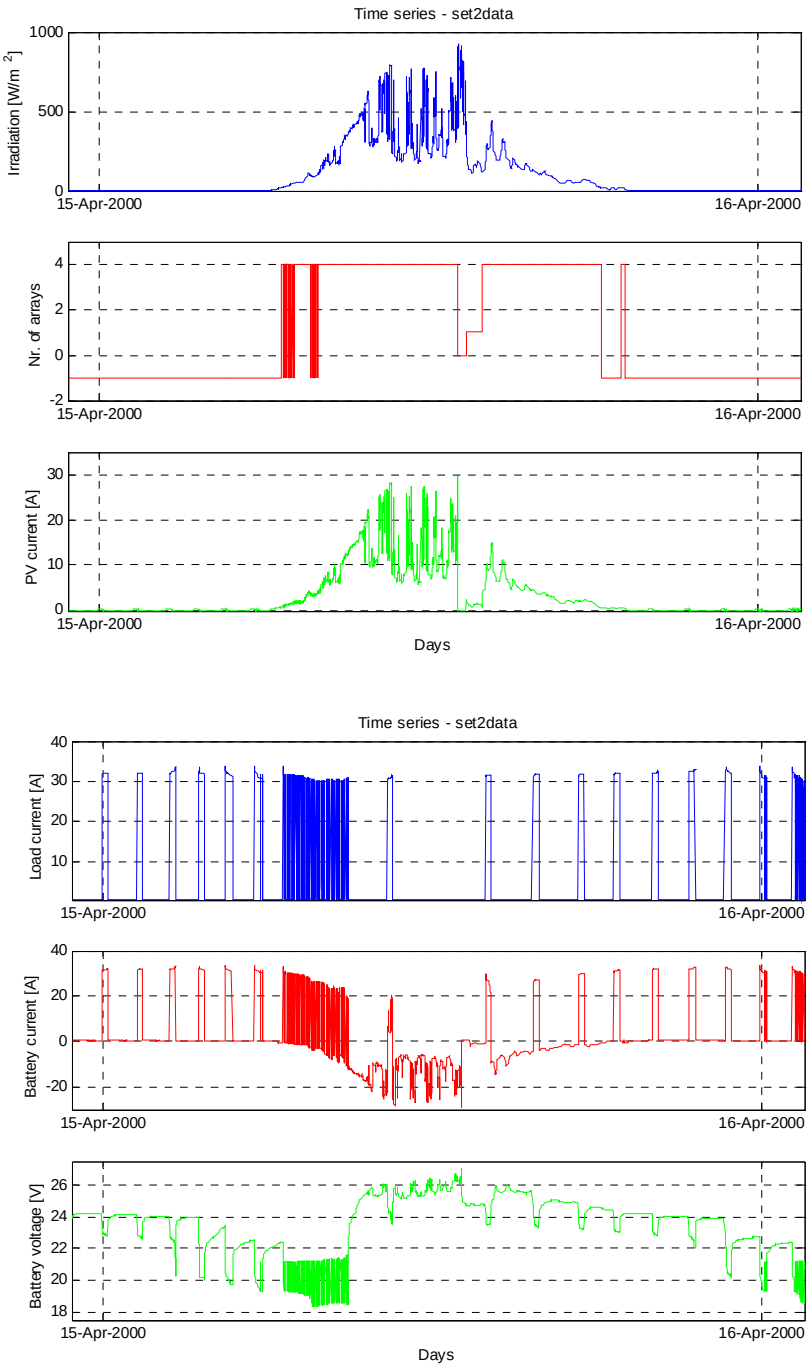

Figure 60: Set2data

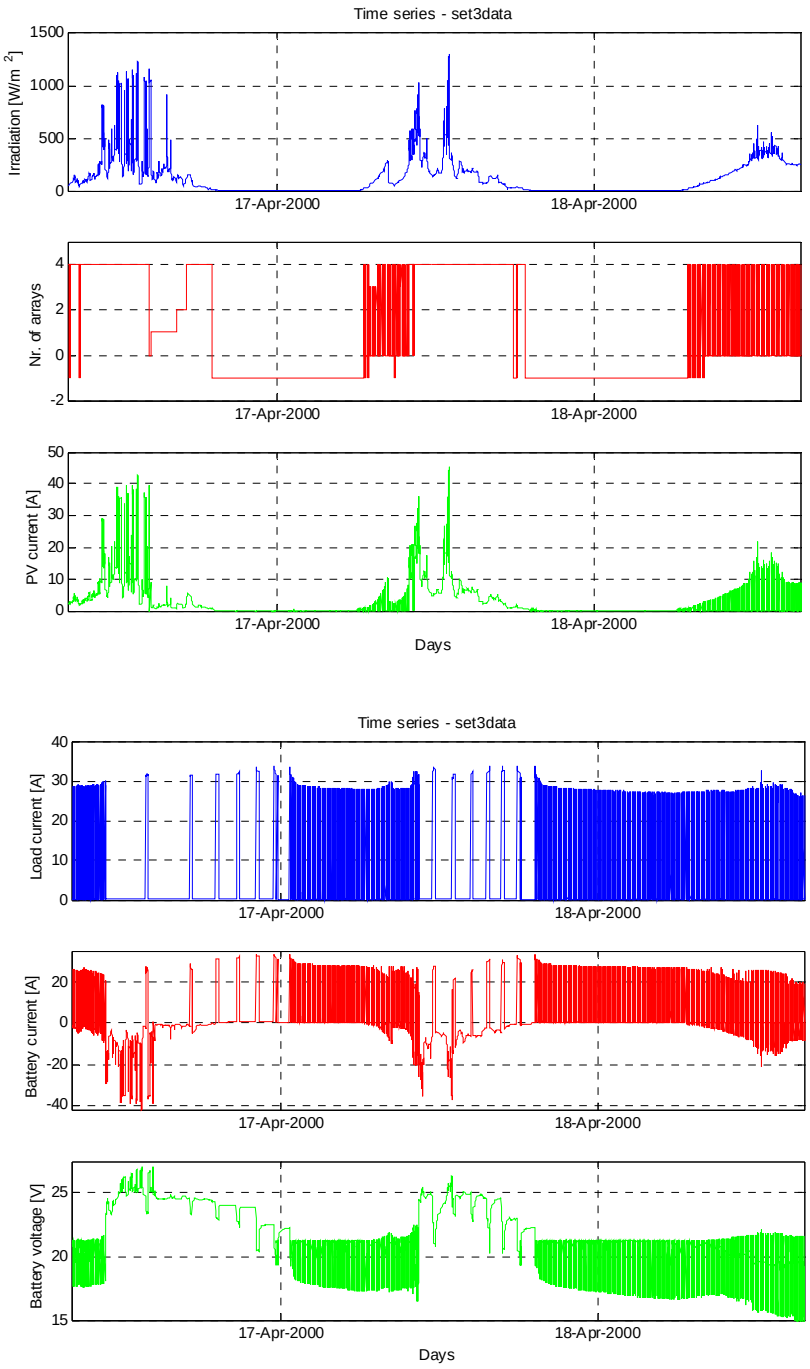

Figure 61: Set3data

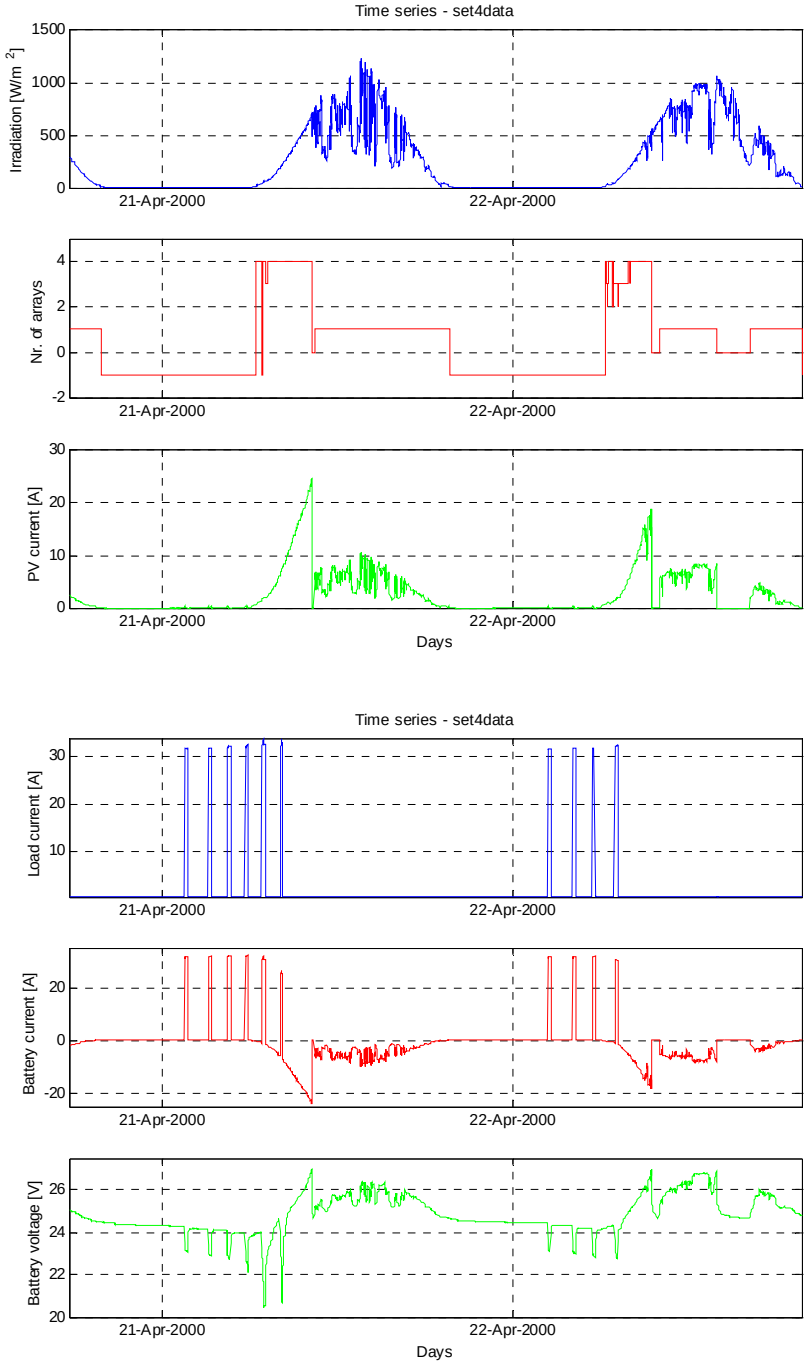

Figure 62: Set4data.

Appendix B: PV module data

Figure 63: Basic data for Solel modules (data sheet as source).

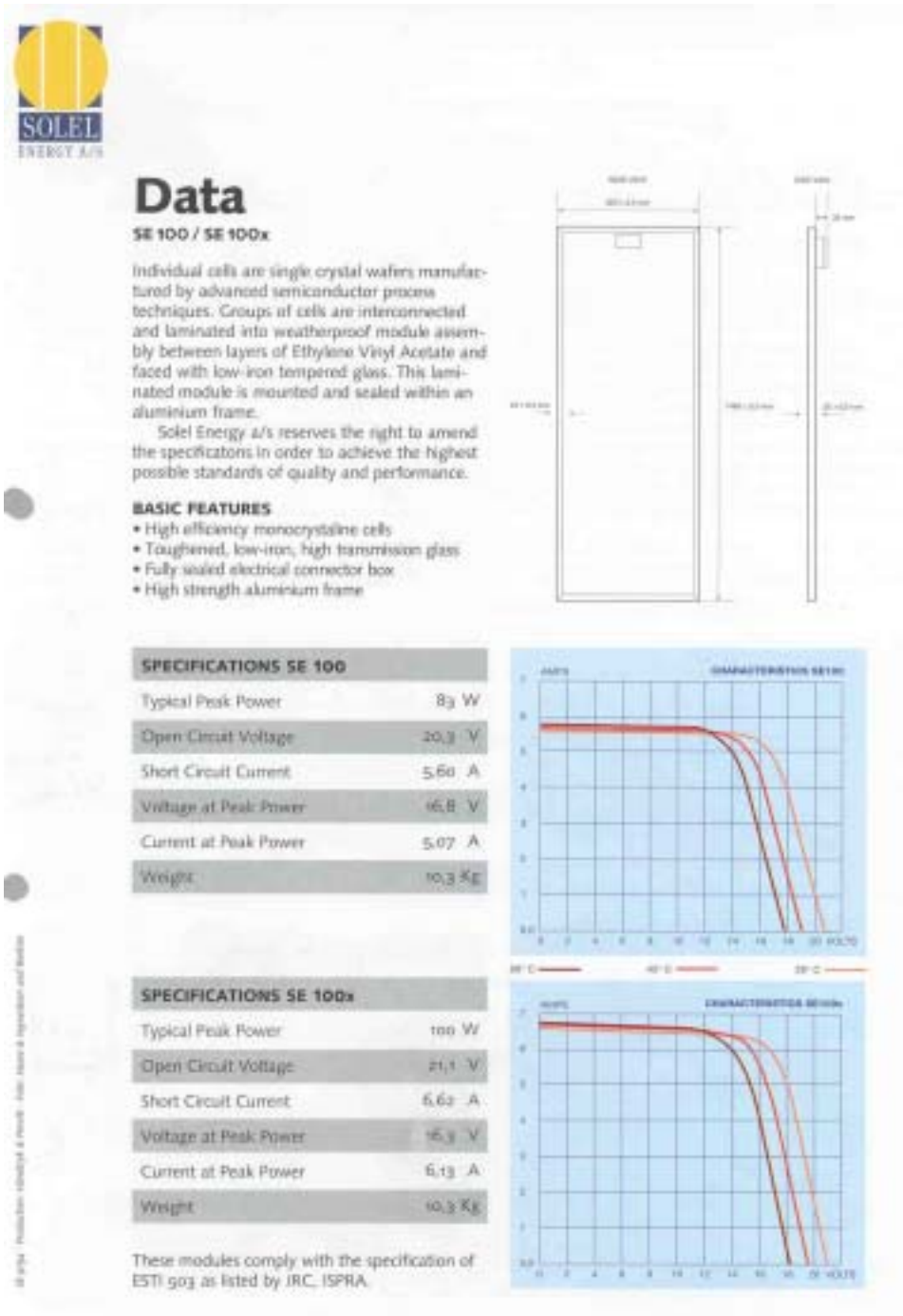

Figure 64: I-V characteristic of the Solel cell (data sheet as source).

Appendix C: PV controller scheme

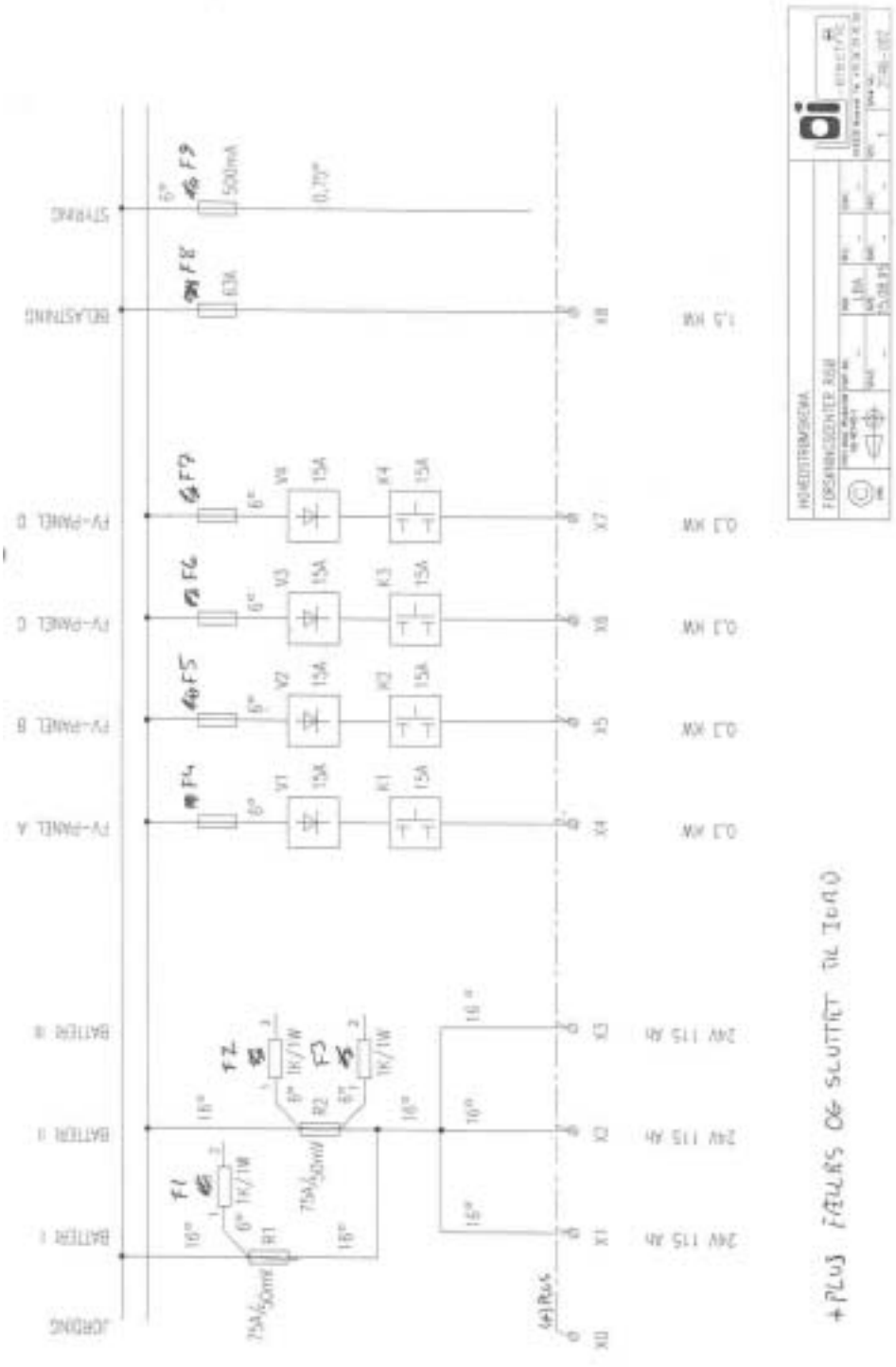

Figure 65: PV controller scheme (data sheet as source).

References

Box, G.E.P., & Jenkins, G.M. (1976). Time series analysis, Forecasting and Control. HoldenDay.

Facinelli, W.A. (1983). Modelling and Simulation of Lead Acid Batteries for Photovoltaic Systems. In Proceedings of the 18th IECEC

Hansen, L.H. (1997). Stochastic modelling of central heating systems. Danish Technical University: PHD-thesis no. IMM-PHD-1997-34,

Holst, J., Madsen, H., & Melgaard, H. (1992). Validation of Grey box models. In Symposium on Adaptive Systems in Control and Signal Processing IFAC, Grenoble, France

Hyman, E., Spindler, W., & Fatula, J.F. (1986). Phenomenological Discharge Voltage Model for Lead Acid Batteries. In Proceedings of AIChe Meeting, Mathematical Modelling of Batteries

Ljung, L. (2000). System identification Toolbox- for use with Matlab. (6 ed.). The Math Works, Inc.

Ljung.L. (1999). System Identification-Theory for the user. Prentice Hall, Upper Saddle River, N.J.2nd.

Lorenzo, E. (1994). Solar Electricity Engineering of Photovoltaic Systems. Artes Graficas Gala, S.L., Spain.

Madsen, H. (1995). Tidsrækkeanalyse (Eng: Time Series Analysis). (2 ed.). Institute of Mathematical Modelling, Danish Technical University.

Manwell, J.F., & McGowan, J.G. (1993). Lead acid battery storage model for hybrid energy systems. Solar Energy, 50(5), 399-405.

Manwell, J.F.,& McGowan, J.G. (1994). Extension of the Kinetic Battery Model for Wind/Hybrid Power Systems. In Proceedings of EWEC 284-289

Manwell, J.F., McGowan, J.G., Baring-Gould, E.I., Stein, W., & Leotta, A. (1994). Evaluation of battery models for wind hybrid power system simulations. In Proceedings of EWEC

Soderstrom, T., & Stoica, P. (1989). System Identification. Prentice Hall International, London.

Bibliographic Data Sheet **Risø-R-1219(EN)/SEC-R-12**

Title and authors

Models for a stand-alone PV system

Anca D. Hansen, Poul Sørensen, Lars H. Hansen and Henrik Bindner

ISBN	ISSN
87-550-2774-1 87-550-2776-8 (Internet)	0106-2840 1600-3780

Department or group	Date
Wind Energy and Atmospheric Physics Department Electrical Design and Control Group	December 2000

Groups own reg. number(s)	Project/contract No(s)

Pages	Tables	Illustrations	References
77	8	65	13

Abstract (max. 2000 characters)

This report presents a number of models for modelling and simulation of a stand-alone photovoltaic (PV) system with a battery bank verified against a system installed at Risø National Laboratory. The work has been supported by the Danish Ministry of Energy, as a part of the activities in the Solar Energy Centre Denmark.

The study is carried out at Risø National Laboratory with the main purpose to establish a library of simple mathematical models for each individual element of a stand-alone PV system, namely solar cells, battery, controller, inverter and load. The models for PV module and battery are based on the model descriptions found in the literature. The battery model is developed at UMASS and is known as the Kinetic Battery Model (KiBaM). The other component models in the PV system are based on simple electrical knowledge. The implementation is done using Matlab/Simulink, a simulation program that provides a graphical interface for building models as modular block diagrams.

The non-linear behaviour of the battery, observed in the measurements, is investigated and compared to the KiBaM model's performance. A set of linear Black box models are estimated based on the battery measurements. The performance of the best linear Black box model is compared to the KiBaM model.

A validation of each of the implemented mathematical model is performed by an interactive analysis and comparison between simulation results and measurements, acquired from the stand-alone PV system at Risø.

Descriptors INIS/EDB

COMPUTERIZED SIMULATION; ELECTRIC BATTERIES; MATHEMATICAL MODELS; ON-SITE POWER GENERATION; PHOTOVOLTAIC POWER SUPPLIES; SOLAR CELLS

Available on request from Information Service Department, Risø National Laboratory,
(Afdelingen for Informationsservice, Forskningscenter Risø), P.O.Box 49, DK-4000 Roskilde, Denmark.
Telephone (+45) 4677 4004, Telefax (+45) 4677 4013